INVENTION OF BIAXIAL LOADING FRAME

FOR INTACT ROCKS

Narit Maneewan

A Thesis Submitted in Partial Fulfillment of the Requirements for the

Degree of Master of Engineering in Geotechnology

Suranaree University of Technology

Academic Year 2012

การประดิษฐ์โครงกดในสองแกนสำหรับตัวอย่างหิน

นายนริศ มณีวรรณ

วิทยานิพนธ์นี้เป็นส่วนหนึ่งของการศึกษาตามหลักสูตรปริญญาวิศวกรรมศาสตรมหาบัณฑิต
สาขาวิชาเทคโนโลยีธรณี
มหาวิทยาลัยเทคโนโลยีสุรนารี
ปีการศึกษา 2555

INVENTION OF BIAXIAL LOADING FRAME FOR INTACT ROCKS

Suranaree University of Technology has approved this thesis submitted in partial fulfillment of the requirements for a Master's Degree.

Thesis Examining Committee

_____

(Assoc. Prof. Kriangkrai Trisarn)

Chairperson

_____

(Assoc. Prof. Dr. Kittitep Fuenkajorn)

Member (Thesis Advisor)

_____

(Dr. Decho Phueakphum)

Member

_____ _____

(Prof. Dr. Sukit Limpijumnong) (Assoc. Prof. Flt. Lt. Dr. Kontorn Chamniprasart)

Vice Rector for Academic Affairs Dean of Institute of Engineering

นริศ มณีวรรณ : การประดิษฐ์โครงกดในสองแกนสำหรับตัวอย่างหิน (INVENTION OF BIAXIAL LOADING FRAME FOR INTACT ROCKS) อาจารย์ที่ปรึกษา : รองศาสตราจารย์ ดร.กิตติเทพ เฟื่องขจร, 78 หน้า.

อุปกรณ์กดทดสอบตัวอย่างหินในสองแกนได้ถูกประดิษฐ์ขึ้นเพื่อหาค่าความแข็งและการเปลี่ยนแปลงรูปร่างของตัวอย่างหินในสองแกน อุปกรณ์ดังกล่าวที่ถูกออกแบบและสร้างขึ้นเพื่อสามารถใช้งานกับโครงกดทดสอบตัวอย่างหินที่มีใช้ทั่วไป ข้อกำหนดของการออกแบบที่สำคัญคือ มีความแข็งแรง ทนทาน ราคาถูก ง่ายต่อการใช้งาน และให้ผลการทดสอบที่สอดคล้องกันกับโครงกดทดสอบในสองแกนแบบมาตรฐาน คานส่งแรงกดสี่ชุดที่ตั้งฉากซึ่งกันและกันใช้ส่งถ่ายแรงในแนวดิ่งจากปลายด้านหนึ่งของคานมาเป็นแรงในแนวระนาบที่ตั้งฉากซึ่งกันและกันมากดตัวอย่างหินที่มีแท่นกดรองรับอยู่ แรงในแนวดิ่งสามารถได้จากโครงกดทดสอบในแกนเดียวที่ใช้กันอยู่ทั่วไปพร้อมกับแม่แรงไฮดรอลิก ความสัมพันธ์ระหว่างแรงในแนวดิ่งและแรงในแนวระนาบได้ถูกคำนวณขึ้นโดยใช้เครื่องตรวจวัดแรงที่มีความแม่นยำสูงประกอบกับลูกเหล็กทรงสี่เหลี่ยมลูกบาศก์ที่ได้ติดมาตรวัดความเครียดไว้ โดยผลการสอบเทียบถูกนำมาใช้ในการหาค่าความเค้นด้านข้างที่กระทำบนตัวอย่างหินในขณะที่แรงในแนวดิ่งเพิ่มขึ้น การเคลื่อนตัวในแนวดิ่งของคานส่งแรง ณ จุดต่างๆ ได้มีการสอบเทียบเพื่อหาความสัมพันธ์กับการเคลื่อนตัวในแนวระนาบของชุดหัวกดทั้งสี่ชุด ผลการทดสอบที่ได้ถูกนำมาใช้คำนวณหาค่าสัมประสิทธิ์ความยืดหยุ่นและอัตราส่วนปัวซองของตัวอย่างหิน การทดสอบทางกลศาสตร์ได้ถูกดำเนินการเพื่อประเมินประสิทธิภาพการทำงานของอุปกรณ์ใหม่ที่ประดิษฐ์ขึ้นโดยการหาค่าความเค้นกดในแกนเดียว ค่าความเค้นกดในสองแกน ค่าสัมประสิทธิ์ความยืดหยุ่นและอัตราส่วนปัวซองของตัวอย่างหินรูปทรงสี่เหลี่ยมลูกบาศก์ขนาด 50×50×50 ลูกบาศก์มิลลิเมตร โดยตัวอย่างหินประกอบด้วย หินทรายชุดพระวิหาร หินทรายชุดภูพาน หินทรายชุดภูกระดึง หินอ่อนชุดสระบุรี และเกลือหินชุดมหาสารคาม การเปลี่ยนแปลงรูปร่างของตัวอย่างหินถูกตรวจวัดทั้งสามทิศทางหลักเพื่อนำมาสร้างกราฟความสัมพันธ์ระหว่างความเค้นกับความเครียด ตัวอย่างหินทั้งหมดได้ถูกนำมาหาค่าความแข็งและค่าความยืดหยุ่นจากการทดสอบโดยใช้โครงกดทดสอบในสองแกนแบบมาตรฐานด้วย การเปรียบเทียบระหว่างผลการทดสอบที่ได้จากอุปกรณ์ที่ได้ประดิษฐ์ขึ้นกับโครงกดทดสอบแบบมาตรฐานระบุว่า ค่ากำลังกดในแกนเดียว กำลังกดในสองแกน และความยืดหยุ่นจากอุปกรณ์ทั้งสองชนิดใกล้เคียงกันมาก

สาขาวิชา เทคโนโลยีธรณี ลายมือชื่อนักศึกษา _____

ปีการศึกษา 2555 ลายมือชื่ออาจารย์ที่ปรึกษา_____

NARIT MANEEWAN : INVENTION OF BIAXIAL LOADING FRAME FOR INTACT ROCKS. THESIS ADVISOR : ASSOC. PROF. KITTITEP FUENKAJORN, Ph.D., P.E., 78 PP.

INTACT ROCK/ BIAXIAL COMPRESSION/ STRENGTH/ LOAD FRAME

A uniaxial-to-biaxial load converter (UBC) has been developed to determine the biaxial compressive strength and deformability of rock specimens. The proposed device has been designed and fabricated for use with most commercially available compression loading frames. The key design requirements are that the new testing device is rugged, inexpensive and easy to operate and that it can provide the results comparable to those of the conventional biaxial load frame. Four cantilever beams set in mutually perpendicular directions are used to transform a vertical load on one end of the beams into two mutually perpendicular lateral loads on the rock specimen via vertical load platens. The vertical load on the UBC can be obtained from any conventional uniaxial load frame equipped with a hydraulic load cell. Calibration curves are developed to correlate the applied vertical load with the lateral loads by using a high precision electronic load cell and a reference cubical steel block attached with two directional strain gages. The calibration results are used to determine the lateral stresses applied on the specimen while the vertical load is increased. The vertical displacement of the cantilever beams at the point where the vertical load is applied is also calibrated with the lateral movement of the four loading platens. The results are used to calculate the elastic modulus and Poisson's ratio of the rock specimen. Series of mechanical tests have been carried out to assess the performance

of the UBC by determining the uniaxial and biaxial compressive strengths, elastic modulus and Poisson's ratio cubical rock specimens with nominal dimensions of 50×50×50 mm^3. The specimens are prepared from Phra Wihan, Phu Phan and Phu Kradung sandstones, Saraburi marble and Maha Sarakham salt. The specimen deformations are monitored along the three principal directions to develop stress-strain curves from start loading until failure. The strengths and elastic parameters of these rocks are also determined by using a conventional biaxial load frame. Comparison of the results obtained from the UBC and the conventional biaxial load frame is made. The results indicate that the uniaxial and biaxial strengths and elastic parameters obtained from the two devices are virtually identical.

School of Geotechnology Student's Signature_____

Academic Year 2012 Advisor's Signature_____

ACKNOWLEDGMENTS

I wish to acknowledge the funding supported by Suranaree University of Technology (SUT).

I would like to express my sincere gratitude thanks to Assoc. Prof. Dr. Kittitep Fuenkajorn for his valuable guidance and efficient supervision. I appreciate for his strong support, encouragement, suggestions and comments during the research period. My heartiness thanks to Assoc. Kriangkrai Trisarn and Dr. Decho Phueakphum for their constructive advice, valuable suggestions and comments on my research works as thesis committee members.

Finally, I would like to thank beloved parents for their love, moral support and constant encouragement.

Narit Maneewan

TABLE OF CONTENTS

Page

TABLE OF CONTENTS (Continued)

Page

TABLE OF CONTENTS (Continued)

Page

LIST OF TABLES

Table **Page**

LIST OF FIGURES

Figure **Page**

LIST OF FIGURES (Continued)

Figure **Page**

LIST OF FIGURES (Continued)

Figure **Page**

SYMBOLS AND ABBREVIATIONS

σ_1	=	maximum principal stress
σ_2	=	intermediate principal stress
σ_3	=	minimum principal stress
ε_1	=	maximum principal strain
ε_2	=	intermediate principal strain
ε_3	=	minimum principal strain
ε_V	=	volumetric strain
C_0	=	uniaxial compressive strength
E_j	=	deformation modulus
J_1	=	the first order of stress invariant
$J_2^{1/2}$	=	the second order of stress invariant
σ_{max}	=	maximum normal stress in the member
M	=	internal moment
c	=	the perpendicular distance from the neutral axis to a point farthest away from the neutral axis
I	=	moment of inertia
P_{cr}	=	critical load capacity of swing arms
E	=	modulus of elasticity
L	=	length of specimen or column
τ_{max}	=	maximum shear stress in the hinge
V	=	shear force

SYMBOLS AND ABBREVIATIONS (Continued)

A	=	cross-sectional area of the hinge
F_h	=	horizontal force
F_v	=	vertical force
d_v/d_h	=	the vertical and horizontal displacement ratio
ε	=	strain
ΔL	=	relative shortening of the specimen length
σ	=	maximum uniaxial stress
ν	=	Poisson's ratio

CHAPTER I

INTRODUCTION

1.1 Background and rationale

Rock deformation and strength are one of the important parameters for the design and stability analysis of geological structures, e.g., foundations of dam, building and bridge, and host rocks for tunnels and underground mines. For underground openings the effects of the confining pressures at the opening boundaries on those properties can be simulated in the laboratory by performing biaxial compression testing of cube-shaped specimens. Obtaining rock strengths in the laboratory under a biaxial stress state is not only difficult but also expensive. Special loading device (e.g. polyaxial loading device) is required. As a result the failure criterion that can take into account the three-dimensional stress states is rare. The existing two dimensional failure criteria for brittle rocks may not be adequate because they are not in the form that can readily be applied in the actual design and analysis of geological structures.

1.2 Research objectives

The objectives of this research involve the design and invention of uniaxial-to-biaxial load converter (hereafter designated as UBC) to test rock specimens under biaxial compressive loadings. The proposed device is designed and fabricated for use with most commercially available compression loading frames. The key design requirements are that the new testing device is rugged, inexpensive and easy to

operate and that it can provide the results comparable to those of the conventional biaxial load frame. Laboratory testing is carried out to assess the performance of the UBC by determining the biaxial compressive strength and deformability of cubical rock specimens. The failure stresses are measured and mode of failure is examined. The research findings not only demonstrate the performance of the new testing device, but also improve our understanding of the biaxial compressive strength of intact rocks.

1.3 Research methodology

The research methodology shown in Figure 1.1 comprises 8 steps; including literature review, design and invention of UBC, fabricating new device, sample preparation, laboratory testing, discussions and conclusions and thesis writing.

1.3.1 Literature review

Literature review is carried out to study the rock deformation and strength in true biaxial stress state, review various types of the biaxial or triaxial load frames. The sources of information are from text books, journals, technical reports and conference papers. The summary of the literature review is given in the thesis.

1.3.2 Design of UBC

The UBC is designed to determine rock strength and deformation under biaxial compressive loading. The device can be used with commonly available load frames. Detailed design and design components are developed.

1.3.3 Fabricating UBC

The UBC is fabricated. It is made of hard steel. Factor of safety for each component is calculated.

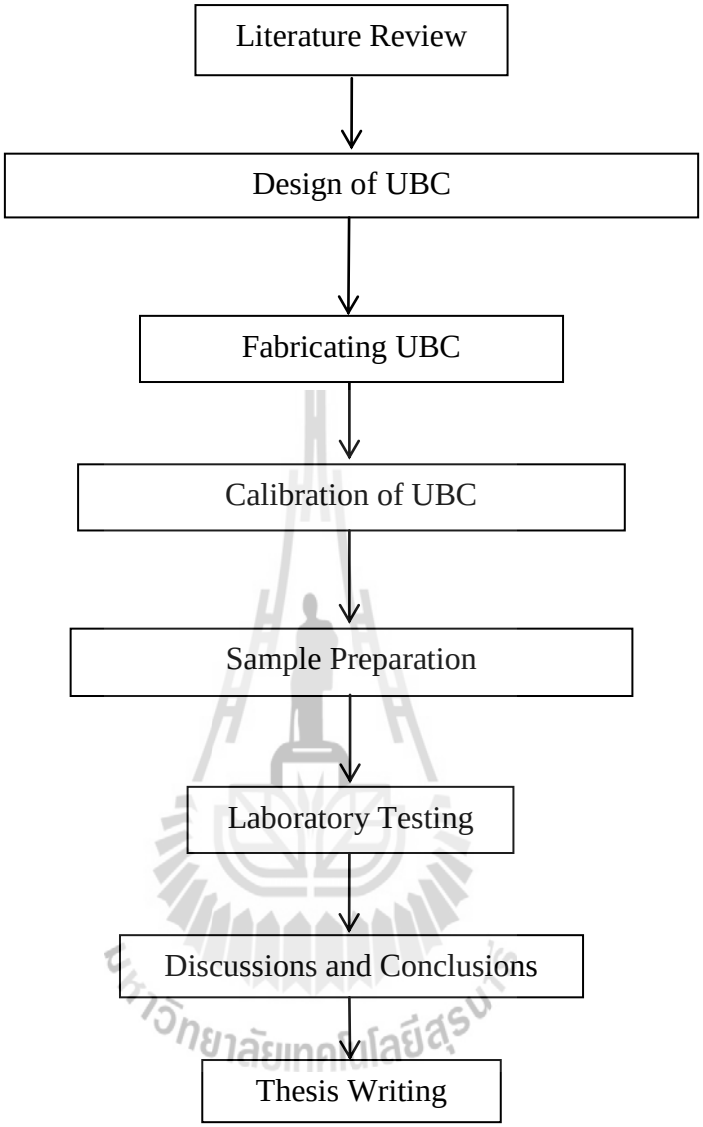

Figure 1.1 Research methodology.

1.3.4 Calibration of UBC

The lateral and axial loads of biaxial testing device are calibrated using electronic load cell. The calibration curves are developed for use in the determination of the lateral stresses and deformation during testing.

1.3.5 Sample preparation

Sample preparation is carried out in the laboratory at the Suranaree University of Technology. The specimens are prepared from Phra Wihan, Phu Phan and Phu Kradung sandstones, Saraburi marble and Maha Sarakham salt. The specimens prepared for compressive strength test have cubic shape with nominal dimensions of $50\times50\times50$ mm^3.

1.3.6 Laboratory testing

Laboratory testing includes biaxial compressive strength tests using UBC and conventional biaxial load frame. Five specimens are tested for each rock type. The specimen deformations are monitored along the three principal directions to develop stress-strain curves from start loading until failure. The strengths and elastic parameters of these rocks are also determined from the conventional biaxial load frame.

1.3.7 Discussions and conclusions

Comparison of the results obtained from the UBC and the conventional biaxial load frame is made in two dimension stress states. Performance of the proposed device is discussed and evaluated.

1.3.8 Thesis writing

All research activities, methods and results are documented and complied in the thesis. The research findings are published in the conference proceedings.

1.4 Scopes and limitations of the study

The scopes and limitations of the research include as follows:

1. Design and invention of UBC for use with conventional uniaxial load frame.
2. Rock specimens with nominal dimensions of 50×50×50 mm^3 are tested to assess the device performance.
3. All tests are conducted under ambient and dry condition.
4. A user manual for the new device is developed.

1.5 Thesis contents

This research thesis is divided into seven chapters. The first chapter includes background and rationale, research objectives, research methodology and scope and limitations. **Chapter II** presents results of the literature review to improve an understanding of rock compressive strength as affected by the intermediate principal stress. **Chapter III** describes design and fabrication of the UBC. **Chapter IV** presents the test method of the UBC. **Chapter V** describes the sample preparation. **Chapter VI** presents the test results. **Chapter VII** gives the discussions, conclusions and recommendations for future studies.

CHAPTER II

LITERATURE REVIEW

2.1 Introduction

Relevant topics and previous research results are reviewed to improve an understanding of rock compressive strengths under biaxial and true triaxial loadings. Summary of the review results is described below.

2.2 True triaxial compressive strength of rock

Wiebols and Cook (1968) investigated the effect of σ_2 on rock strength, based on the earlier testing results. Early attempts to examine the influence of σ_2 on rock strength were made in 1960s by Murrell (1963) and Handin et al. (1967). They compared the results from a series of triaxial tests conducted in marble, limestone, dolomite, and glass [triaxial compression tests ($\sigma_1 > \sigma_2 = \sigma_3$) and triaxial extension test ($\sigma_1 = \sigma_2 > \sigma_3$)] and noted that the rock strength for any given σ_3 was larger in triaxial extension than in triaxial compression, thus suggesting that the intermediate principal stress does, in fact, affect mechanical properties. Handin et al. (1967) carried out several triaxial compression and triaxial extension tests in Solenhofen limestone, Blaire dolomite and Pyrex glass. They obtained results similar to those of Murrell's showing that rock strength was higher when the larger intermediate principal stress ($\sigma_2 = \sigma_1$) was applied. Based on these earlier experimental results, Wiebols and Cook (1968) pursued a theoretical approach to further investigate the

effect of σ_2 on rock strength. They derived a strength criterion based on the strain energy stored by the rock in the absence of discontinuities, and the additional strain energy around Griffith cracks as a result of sliding of crack surfaces over each other. They found that under true triaxial (polyaxial) compressive stress conditions the intermediate principal stress has a pronounced effect, predictable if the coefficient of sliding friction between crack surfaces is known.

In particular, Wiebols and Cook (1968) determined from their model that if σ_3 is held constant and σ_2 is increased from $\sigma_2 = \sigma_3$ to $\sigma_2 = \sigma_1$ the strength first increases, reaches a maximum at some value of σ_2 and then decreases to a level higher than that obtained in a triaxial test, i.e. when $\sigma_2 = \sigma_3$.

Wawersik et al. (1997) develop the true-triaxial apparatus (Figure 2.1) that makes use of conventional triaxial pressure vessels in combination with specially configured, high-pressure hydraulic jacks inside these vessels. The development combines advantages not found in existing facilities, including a compact design, pore-pressure and flow-through capabilities, the ability to attain high principal stresses and principal stress differences, direct access to parts of the sample, and provisions to relatively large deformations without developing serious stress field in homogeneities.

Colmenares and Zoback (2002) examine seven different failure criteria by comparing them to published polyaxial test data ($\sigma_1 > \sigma_2 > \sigma_3$) for five different rock types at a variety of stress states. They employed a grid search algorithm to find the best set of parameters that describe failure for each criterion and the associated misfits. Overall, they found that the polyaxial criterion of Modified Wiebols and Cook and Modified Lade achieved a good fit to most of the test data. This is especially true

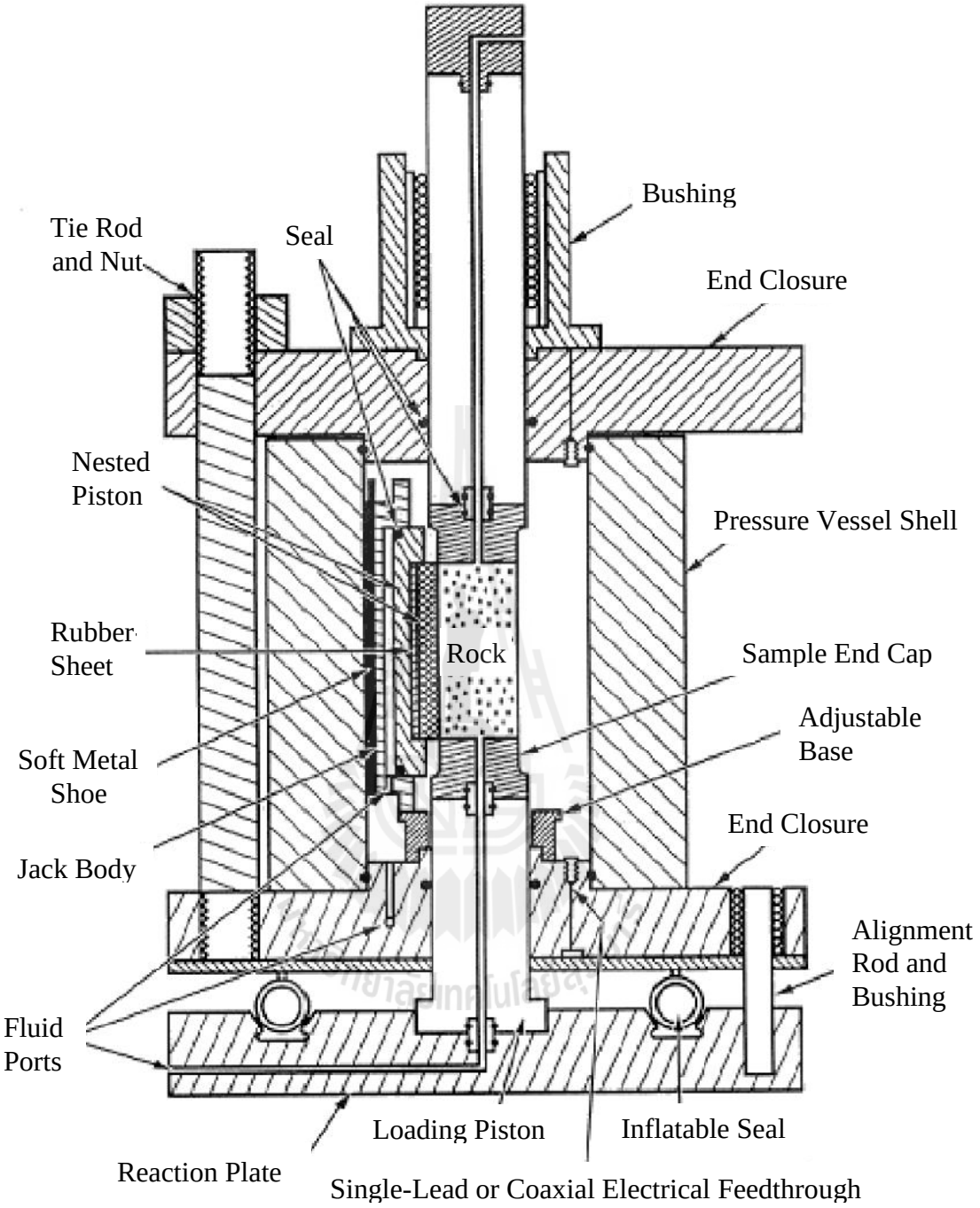

Figure 2.1 Sandia true-triaxial testing system with "floating" pressure vessel shell (Wawersik et al., 1997).

for rocks with a highly σ_2-dependent failure behavior (e.g. Dunham dolomite, Solenhofen limestone). However, for some rock types (e.g. Shirahama Sandstone, Yuubari shale), the intermediate stress hardly affects failure and the Mohr–Coulomb and Hoek and Brown criteria fit these test data equally well, or even better, than the more complicated polyaxial criteria. The values of C_0 (uniaxial compressive strength) yielded by the Inscribed and the Circumscribed Drucker–Prager criteria bounded the C_0 (uniaxial compressive strength) value obtained using the Mohr–Coulomb criterion as expected. In general, the Drucker–Prager failure criterion did not accurately indicate the value of σ_1 at failure. The value of the misfits achieved with the empirical 1967 and 1971 Mogi criteria were generally in between those obtained using the triaxial and the polyaxial criteria. The disadvantage of these failure criteria is that they cannot be related to strength parameters such as C_0: They also found that if only data from triaxial tests are available, it is possible to incorporate the influence of σ_2 on failure by using a polyaxial failure criterion. The results for two out of three rocks that could be analyzed in this way were encouraging.

Kwasniewski et al. (2003) use prismatic samples of medium-grained sandstone from Śląsk Colliery for testing under uniaxial compression, conventional triaxial compression and true triaxial compression conditions. Results of the studies show that confining pressure strongly inhibited dilatant behavior of rock samples tested under conventional triaxial compression conditions; the increasing confinement resulted in the growing compaction of the rock material. The effect of dilatancy was also highly suppressed by the intermediate principal stress. While important dilatant, negative volumetric strain corresponded to the peak differential stress at low intermediate principal stress conditions, at high intermediate stresses the rock

material was damaged to much lesser extent. As a result, faulting of rock samples in the post-peak region was much more violent and was accompanied by a strong acoustic effect.

Alexeev et al. (2004) present two generations of true triaxial loading (TTAL) apparatus. First generation was intended primarily for true stress state imitation in rock or mineral specimens. Advanced second-generation is designed to provide precise measurements in any stress and simulation of rock outburst at sudden relief of one sample face. Both TTAL apparatuses can apply pressure up to 250 MPa, corresponding to earth depth about 10,000 m, independently along each of three axes. Experimental results are given on effect of absorbed water on ultimate state in coal as well as adsorbed methane influence on simulated coal outbursts.

Tiwari and Rao (2004) described physical modeling of a rock mass under a true triaxial stress state by using block mass models having three smooth joint sets. The testing used true-triaxial system (TTS) developed by Rao and Tiwari (2002), shown in Figure 2.2. The test results show the strength of rock mass (σ_1) and deformation modulus (E_j) increase significantly which is confirmed by fracture shear planes developed on σ_2 face of specimen. Most of the specimens failed in shearing with sliding in some cases. The effect of interlocking and rotation of principal stresses σ_2 and σ_3 on strength and deformation response was also investigated.

Chang and Haimson (2005) discuss the non-dilatants deformation and failure mechanism under true triaxial compression. They conducted laboratory rock strength experiments on two brittle rocks, hornfels and metapelite, which together are the major constituent of the long valley Caldera (California, USA) basement in the

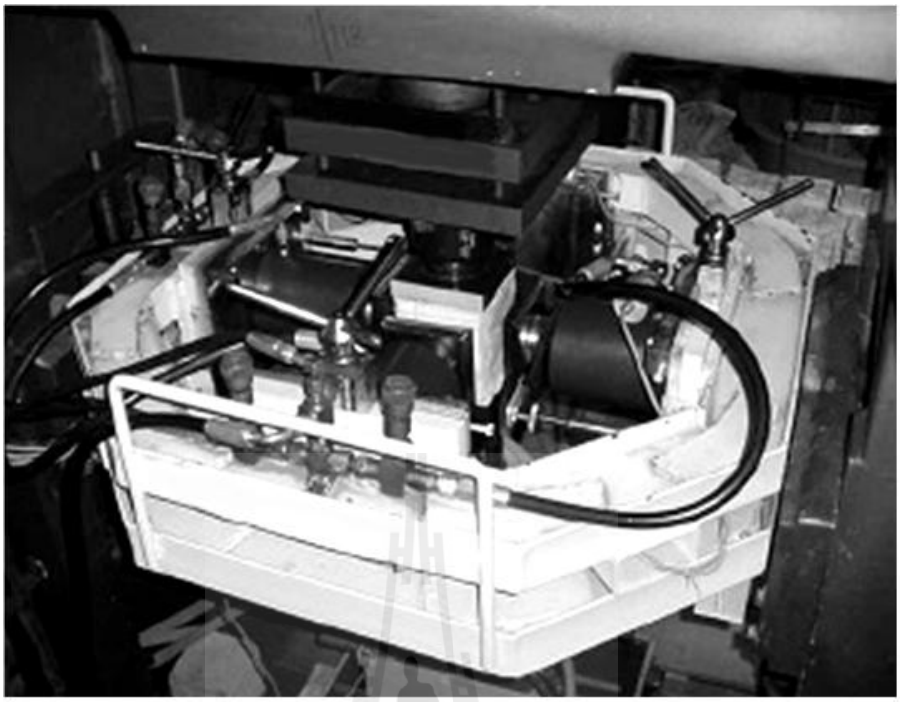

Figure 2.2 True triaxial system used for study (Rao and Tiwari, 2002).

2025 – 2996 m depth range. Both rocks are banded, very high porosity. Uniaxial compression test at different orientations with respect to banding planes reveal that the hornfels compressive strength nearly isotropic, the metapelite possesses distinct anisotropy. Conventional triaxial tests in these rocks reveal that their respective strengths in a specific orientation increase approximately linearly with confining pressure. True triaxial compressive experiments in specimens oriented at a consistent angle to banding, in which the magnitude of the least (σ_3) and the intermediate (σ_2) principal stress are different but kept constant during testing while the maximum principal stress is increased until failure, exhibit a behavior unlike that previously observed in other rocks under similar testing conditions. For a given magnitude of σ_3, compressive strength σ_1 does not vary significantly in both regardless of the applied σ_2, suggesting little or no intermediate principal stress effect. Strains measured in all

three principal directions during loading were used to obtain plots σ_1 versus volumetric strain. These are consistently linear almost to the point of rock failure, suggesting no dilatants.

Haimson (2006) describes the effect of the intermediate principal stress (σ_2) on brittle fracture of rocks, and on their strength criteria. Testing equipment emulating Mogi's but considerably more compact was developed at the University of Wisconsin and used for true triaxial testing (Figure 2.3) of some very strong crystalline rocks. Test results revealed three distinct compressive failure mechanisms, depending on loading mode and rock type: shear faulting resulting from extensile microcrack localization, multiple splitting along the axis, and nondilatant shear failure. The true triaxial strength criterion for the KTB amphibolite derived from such tests was used in conjunction with logged breakout dimensions to estimate the maximum horizontal in situ stress in the KTB ultra deep scientific hole.

Tiwari and Rao (2006) provide results of triaxial and true triaxial testing conducted on physical models of a rock mass to describe its post failure behavior. The testing was performed using a True Triaxial System (TTS) developed by the authors. The results show estimate post peak modulus in triaxial and true triaxial stress conditions.

Cai (2008) studied the intermediate principal stress on rock fracturing and strength near excavation boundaries using a FEM/ DEM combined numerical tool. A loading condition of $\sigma_3 = 0$ and $\sigma_1 \neq 0$, and $\sigma_2 \neq 0$ exists at the tunnel boundary, where σ_1, σ_2, and σ_3, are the maximum, intermediate, and minimum principal stress components, respectively. The numerical study is based on sample loading testing

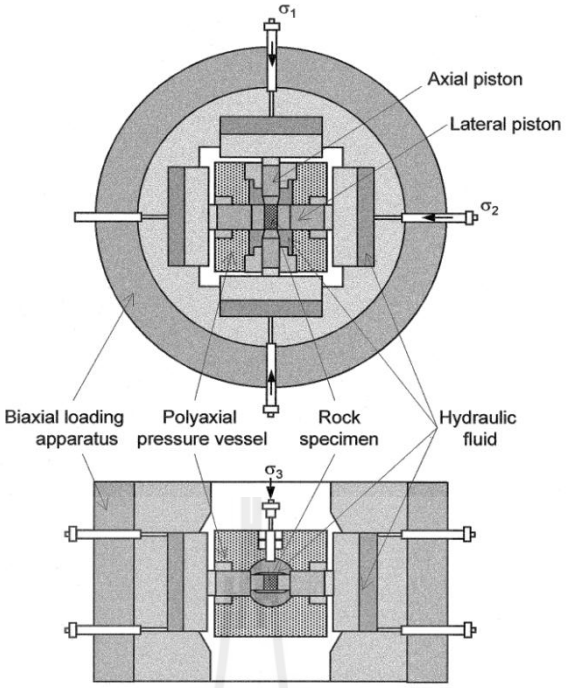

Figure 2.3 Schematic diagram of true triaxial testing system (Haimson and Chang, 2000).

that follows this type of boundary stress condition. It is seen from the simulation principal stress (σ_2), as well as zero to low minimum principal stress (σ_3) confinement. A high intermediate principal stress confines the rock in such away that microcracks and fractures can only be developed in the direction parallel to σ_1 and σ_2. Stress-induced fracturing and microcracking in this fashion can lead to onion-skin fractures, spalling, and slabbing in shallow ground near the opening and surface parallel microcracks further away from the opening, leading to anisotropic behavior of the rock. Consideration of the effect of the intermediate principal stress on rock behavior should focus on the stress-induced anisotropic strength and deformation behavior of the rocks show in Figure 2.4. It is also found that the intermediate principal stress has limited influence on the peak strength of the rock near the excavation boundary.

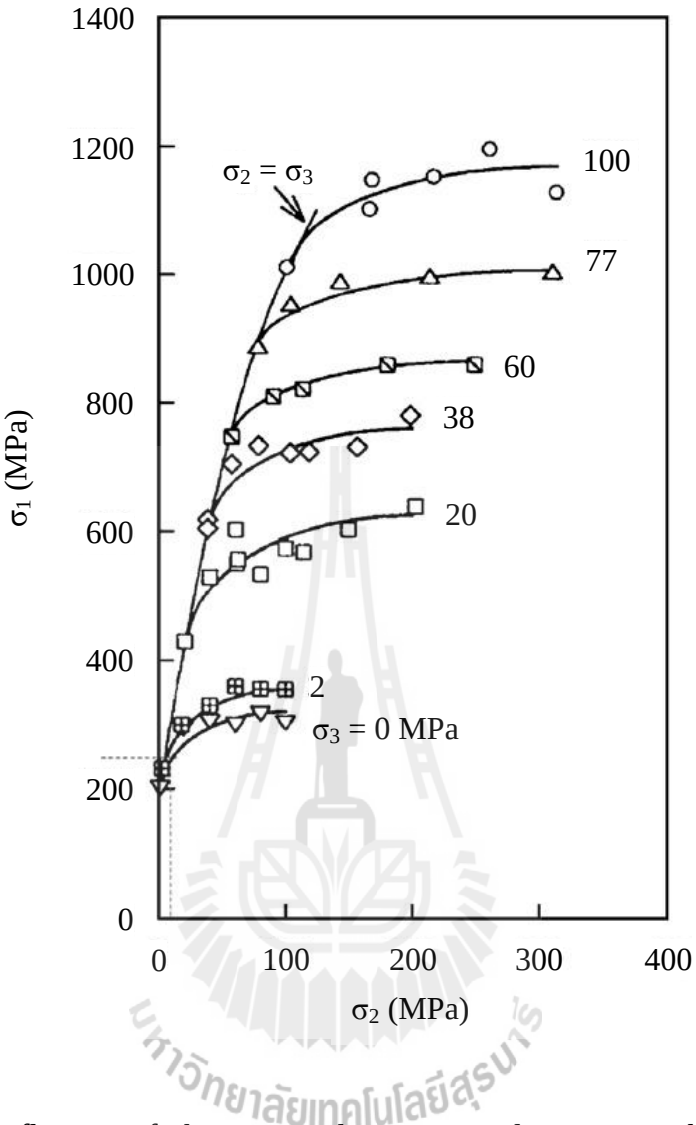

Figure 2.4 Influence of the intermediate principal stress on the strength of Westerly granite. Rapid initial rock strength increases with increasing σ_2 can be seen for low σ_3 (Cai, 2008).

Walsri et al. (2009) developed polyaxial load frame (Figure 2.5) to determine the compressive and tensile strengths of three types of sandstone under true triaxial stresses. Results from the polyaxial compression tests on rectangular specimens of sandstones suggest that the rocks are transversely isotropic.

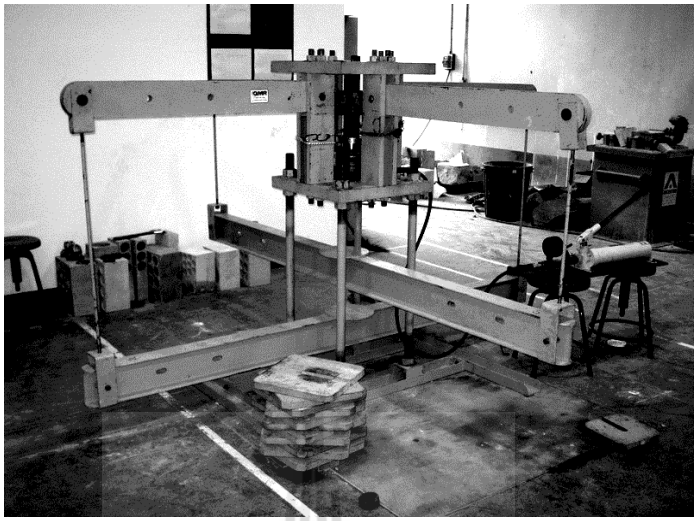

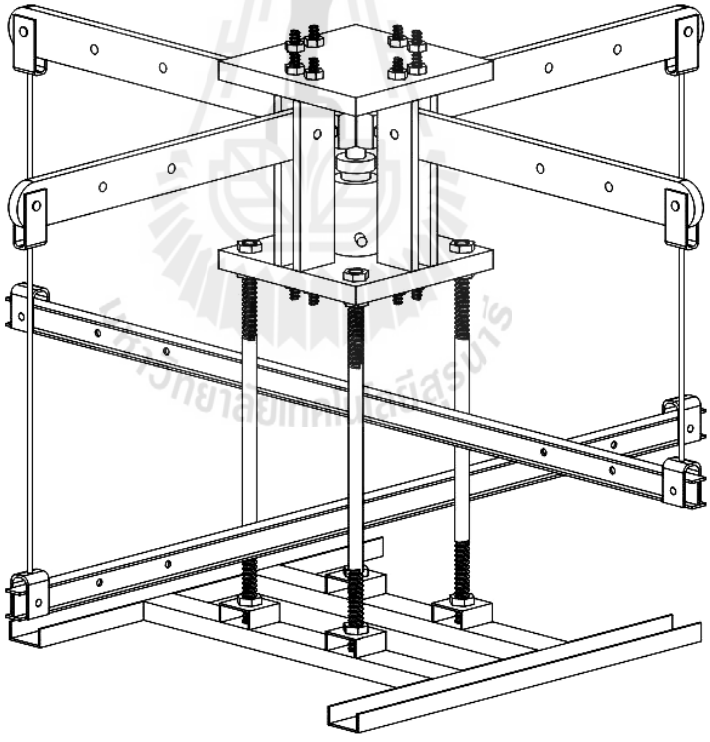

Figure 2.5 Polyaxial load frame developed for rock testing under true triaxial stresses (Walsri et al., 2009).

The measured elastic modulus in the direction parallel to the bedding planes is slightly greater than that normal to the bed. Poisson's ratio on the plane normal to the bedding planes is lower than those on the parallel ones. Under the same σ_3, σ_1 at failure increases with σ_2. Results from the Brazilian tension tests under axial compression reveal the effects of the intermediate principal stress on the rock tensile strength. The Coulomb and modified Wiebols and Cook failure criteria derived from the characterization test results predict the sandstone strengths in term of $J_2^{1/2}$ as a function of J_1 under true triaxial stresses. The modified Wiebols and Cook criterion describes the failure stresses better than does the Coulomb criterion when all principal stresses are in compressions. When the minimum principal stresses are in tension, the Coulomb criterion over-estimate the second order of the stress invariant at failure by about 20% while the modified Wiebols and Cook criterion fails to describe the rock tensile strengths.

Sriapai et al. (2011) have used polyaxial load frame to determine true triaxial compressive strength of Maha Sarakham (MS) salt. The load frame equipped with two pairs of cantilever beam is used to apply the constant lateral stress (σ_2 and σ_3) to salt specimen while the axial stress (σ_1) is increased at 0.5-1.0 MPa/s until failure occurs. The deformations induced along the three loading directions are monitored and used to calculate the tangent elastic modulus and Poisson's ratio of the salt. For the Coulomb criterion the internal friction angle determined from the triaxial loading condition ($\sigma_2=\sigma_3$). The effect of σ_2 on the salt strengths can be best described by the modified Wiebols and Cook criterion. The empirical (power law) Mogi criterion tends to underestimate the salt strengths particularly under high σ_3 values. The modified Lade criterion overestimates the actual strengths at all levels of σ_3. The

Coulomb and Hoek and Brown criteria can not describe the salt strengths beyond the condition where $\sigma_2 = \sigma_3$, as they can not incorporate the effects of σ_2. Both circumscribed and inscribed Drucker-Prager criteria severely underestimate σ_1 at failure for all stress conditions.

2.3 Biaxial compressive strength of rock

Song and Haimson (1997) conducted laboratory simulation tests of borehole breakouts and investigated their potential use as an indicator of in situ stress magnitudes in Westerly granite and Berea sandstone. They also carried out simple triaxial tests and used the results to derive several strength criteria for these rocks. Truly triaxial strength criteria, which incorporate the effect of the intermediate principal stress on failure, are much more in agreement with the stress at the breakout boundary. One such criterion due to Nadai and another due to Mogi, appear suitable for determining breakout failure in the sandstone and the granite. Thin-section analysis suggests that breakout failure mechanism may play an important role in determining the appropriate strength criterion for a given rock type.

Bobet et al. (1998) described fracture coalescence, which plays an important role in the behavior of brittle materials, is investigated by loading pre-fractured specimens of gypsum, used as a rock model material, in uniaxial and biaxial compression. The biaxial testing machine consists of an existing 200 kip Baldwin machine for the major (vertical) load application and a specifically developed, horizontal loading frame for the confining (horizontal) load. The frame has a 100 kN instron actuator and a 50 kN load cell, as shown in Figure 2.6. The horizontal actuator and the Baldwin machine are powered by the Baldwin oil pump, and are

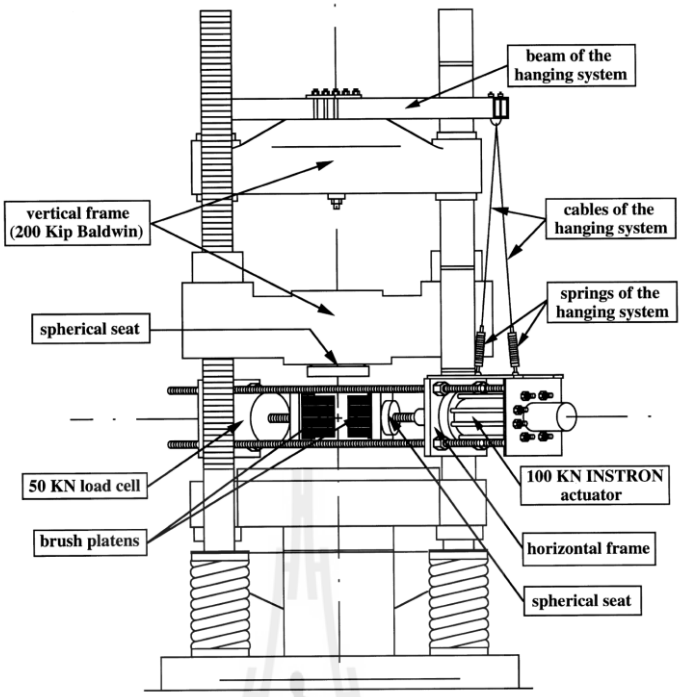

Figure 2.6 Biaxial testing equipment, front view general set-up (Bobet et al., 1998).

feedback controlled by a computer and a software program written for this purpose. Several new phenomena and their dependence on geometry and other conditions are observed. The specimens have two pre-existing fractures or flaw that are arranged in different geometries, and that can be either open or closed. Two different test series are performed with these aw geometries, one under uniaxial loading and one with biaxial loading in which confining stresses of 2.5, 5.0, 7.5 and 10 MPa are applied. As the vertical (axial) load is increased, new cracks emanate from the flaws and eventually coalesce. Flaw slippage, wing crack initiation, secondary crack initiation, crack coalescence, and failure are observed. Two types of cracks occur: wing cracks, which are tensile cracks, and secondary cracks which initiate as shear cracks in a plane roughly co-planar with the flaw. The secondary cracks usually propagate as shear cracks in the same plane but, depending on the geometry, they also propagate

out of plane as either tensile or shear cracks. The wing cracks initiate at the flaw tips for uniaxial or low confinement biaxial conditions but move to the middle of the flaw and disappear completely for higher confining stresses. Three types of coalescence, which depend on the geometry of the flaws and to some extent on stress conditions, occur; they can be distinguished by different combinations of wing cracks and secondary cracks. For closed flaw specimens, at least partial debonding and slippage of the flaws is required prior to initiation of a crack. In uniaxial compression coalescence and failure occur simultaneously, while failure in biaxial compression occurs after coalescence.

Alsayed (2002) used hollow cylinder specimens for simulating stress condition around the opening to study the behaviour of rock under a much wider variety of stress paths. The hollow cylinder specimens are used in conventional triaxial test cell, shown in Figure 2.7. It was developed by Hoek and Franklin (1970) and specially designed of internal of pressure loading configuration. Springwell sandstone specimens were subjected to under uniaxial, biaxial, triaxial and polyaxial compression, as well as indirect tension. The results obtained confirm the effect of the intermediate principal stress on rock failure and show that the apparent strength of rock is markedly influenced by the stress condition imposed. Multiaxial testing system can provide realistic prediction of the actual behaviour of rock and guide the formulation of more adequate numerical models.

Fakhimi et al. (2002) present the simulation of failure around a circular opening in rock. A biaxial compression test was performed on a sandstone specimen with a circular opening to simulate a loading-type failure around an underground excavation in brittle rock, as shown in Figure 2.8. The axial force and displacements

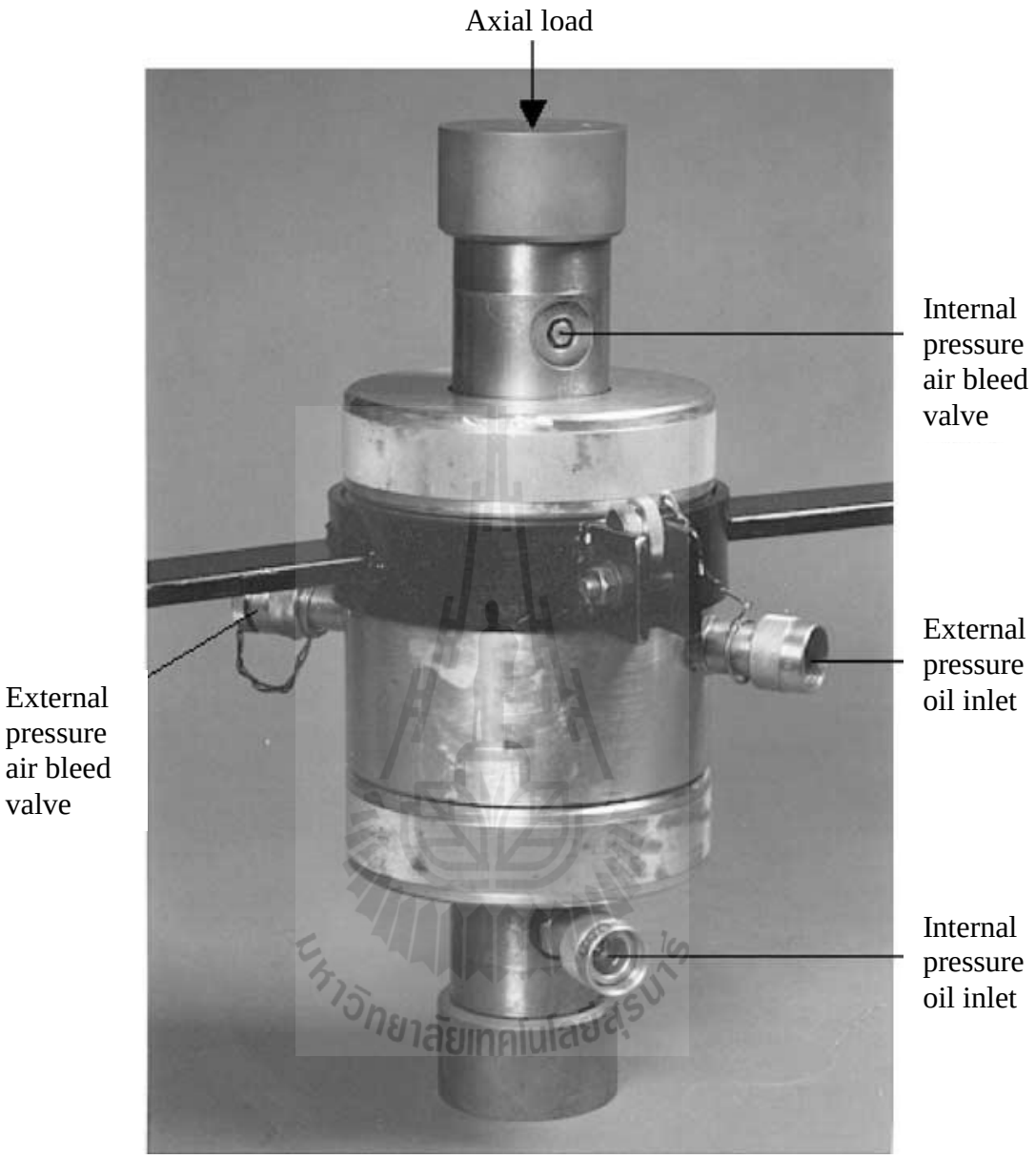

Figure 2.7 Test cell with a specimen inside ready to be transferred to the loading machine (Alsayed, 2002).

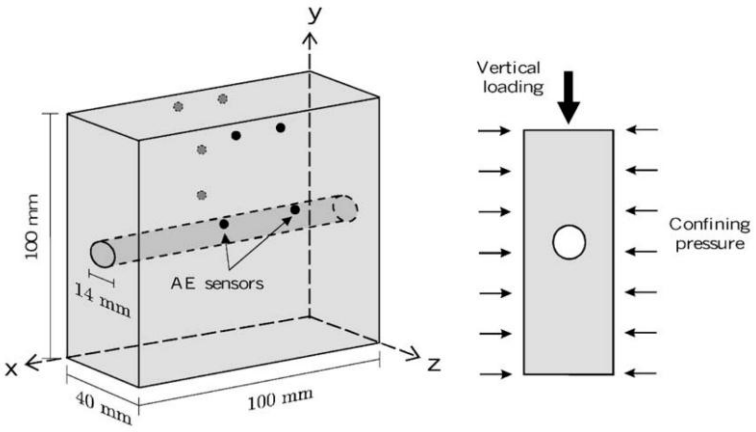

Figure 2.8 Specimen geometry and loading configuration (Fakhimi et al., 2002).

were monitored throughout the failure process, and microcracking was detected by the acoustic emission technique. To model the observed damage zone around the opening, the distinct element computer program, particle flow code (PFC^{2D}), was used. The numerical model consisted of several circular elements that can interact through contact stiffness, exhibit strength through contact bonds and particle friction, and develop damage through fracture of bonds. For the determination of micro-mechanical parameters needed in the calibration process of the computer program, only the macroscopic parameters of Young's modulus, Poisson's ratio and uniaxial compressive strength were used. It is shown that PFC^{2D} was capable of simulating the localization behavior of the rock and the numerical model was able to reproduce the damage zone observed in the laboratory test.

Sahouryeh et al. (2002) described an experimental and analytical investigation into three-dimensional crack growth under biaxial compression is presented. Tests were carried out on different materials, including transparent resin samples, each with a single embedded disk-like crack. These cracks grew extensively

parallel to the load directions causing splitting, shown in Figure 2.9. This behavior is markedly different from that observed under uniaxial compression where the crack growth is limited in size, and is not capable on its own to induce failure. The presence of the intermediate principal compressive stress radically changes the mechanism of crack growth. A model is proposed where the growing crack is represented as a disk-like crack oriented parallel to the loading direction and opened by a pair of concentrated forces at its center. It is shown that the crack growth is stable until it reaches a size comparable to its distance from the free surface.

Zhu et al. (2005) present the simulation of progressive fracturing processes around underground excavations under biaxial compression. Fractures that develop progressively around underground excavations can be simulated using a numerical code called RFPA (rock failure process analysis). The results of the simulations show that the code can be used not only to produce fracturing patterns similar to those reported in previous studies, but also to predict fracturing patterns under a variety of loading conditions. Based on these fracturing patterns, failure mechanisms are identified for various loading conditions.

Kulatilake et al. (2006) conducted experiments for the research: A new rock mass failure criterion for biaxial loading conditions. They investigated the model materials simulating brittle rocks, a mixture of glastone, sand and water. Thin galvanized sheets of thickness 0.254 mm were used to create joints in blocks made out of model material. To investigate the failure modes and strength, both the intact material blocks as well as jointed model material blocks of size 35.6x17.8x2.5 cm having different joint geometry configurations were subjected to uniaxial and biaxial compressive loadings. A new intact rock failure criterion is proposed at the 3-D level.

Figure 2.9 Splitting of concrete sample under biaxial compression (Sahouryeh et al., 2002).

This criterion is validated for biaxial loading through laboratory experimental results obtained on intact model material blocks. Results obtained from both the intact and jointed model material blocks are used to develop a strongly non-linear new rock mass failure criterion for biaxial loading. The equipment for biaxial loading is shown in the below Figures 2.10 and 2.11, including the typical frame used in making the jointed specimens of the model material, as show in Figure 2.12.

Yun et al. (2010) described the biaxial tests of granite cubes of size of 75, 100 and 125 mm. Testing was done with a newly developed biaxial test apparatus, housed in the structural engineering laboratory of Henan Polytechnic University, China. It has a capacity of 500 metric tons in each direction and is equipped with servo-controlled load and displacement systems. Loading rate can be anywhere between 1.25 and 125 kN/s, and displacement rate can range from 4 to 30 μm/s. The availability of high loading rate has permitted the examination of the quasidynamic

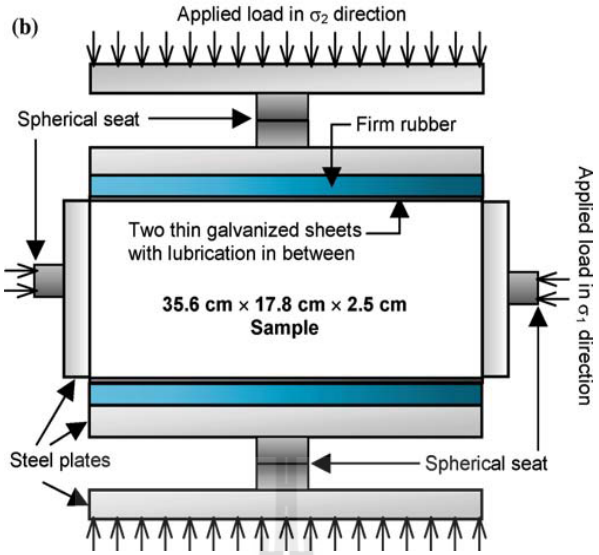

Figure 2.10 A detailed view around the sample under biaxial compression (Kulatilake et al., 2006).

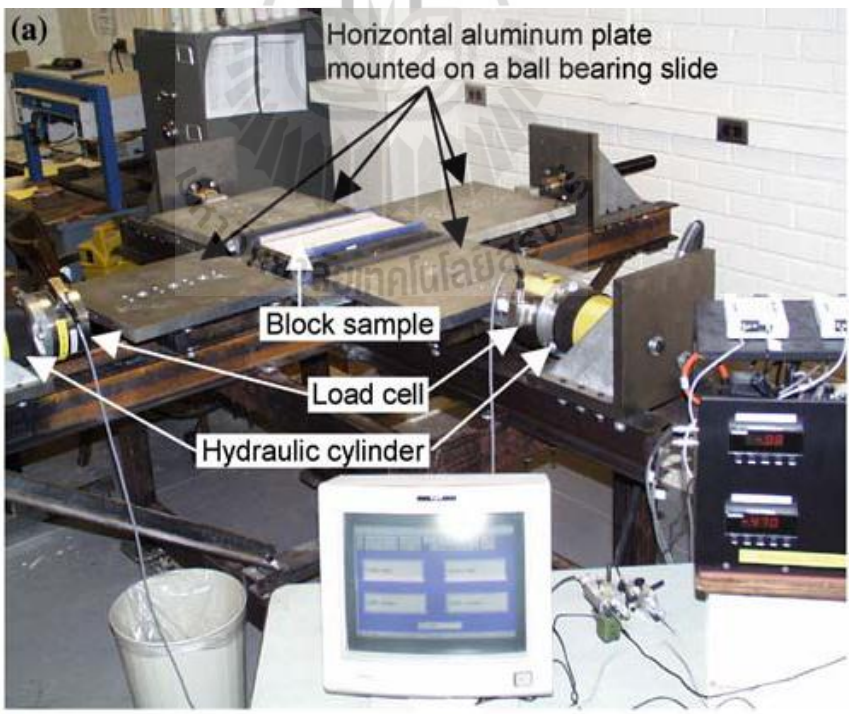

Figure 2.11 Equipment and the data acquisition system used in performing uniaxial and biaxial compression experiments (Kulatilake et al., 2006).

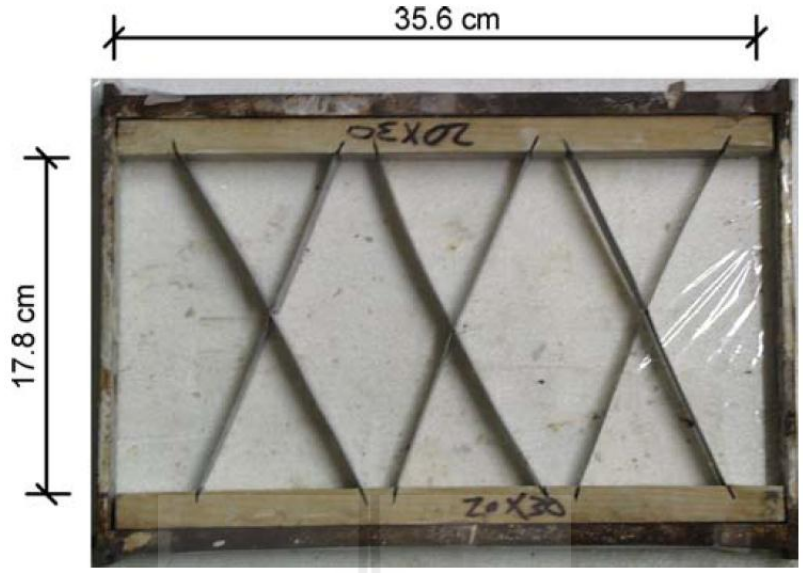

Figure 2.12 Typical frame used in making the jointed specimens of the model material (Kulatilake et al., 2006).

response of granite to sudden load application, as in the case of drift heading excavated by blasting. The failure mechanisms of granite samples show in Figure 2.13.

Both Mohr-Coulomb (Jaeger and Cook, 1979) and Hoek-Brown (1988) criteria neglect the effect of intermediate principal stress σ_2. It can be concluded that while both Mohr-Coulomb and Hoek-Brown failure criteria have many useful applications in practice, they are not suitable for the case of biaxial loading or plane stress.

Sagong et al. (2011) experimented in rock fracture and joint sliding behaviors of jointed rock masses with an opening under biaxial compression which are investigated through experimental and numerical analyses to study in the tunnel construction in rock mass produces damage around the tunnel by concentration of in-situ stress and by construction activity such as blasting. The generated damage

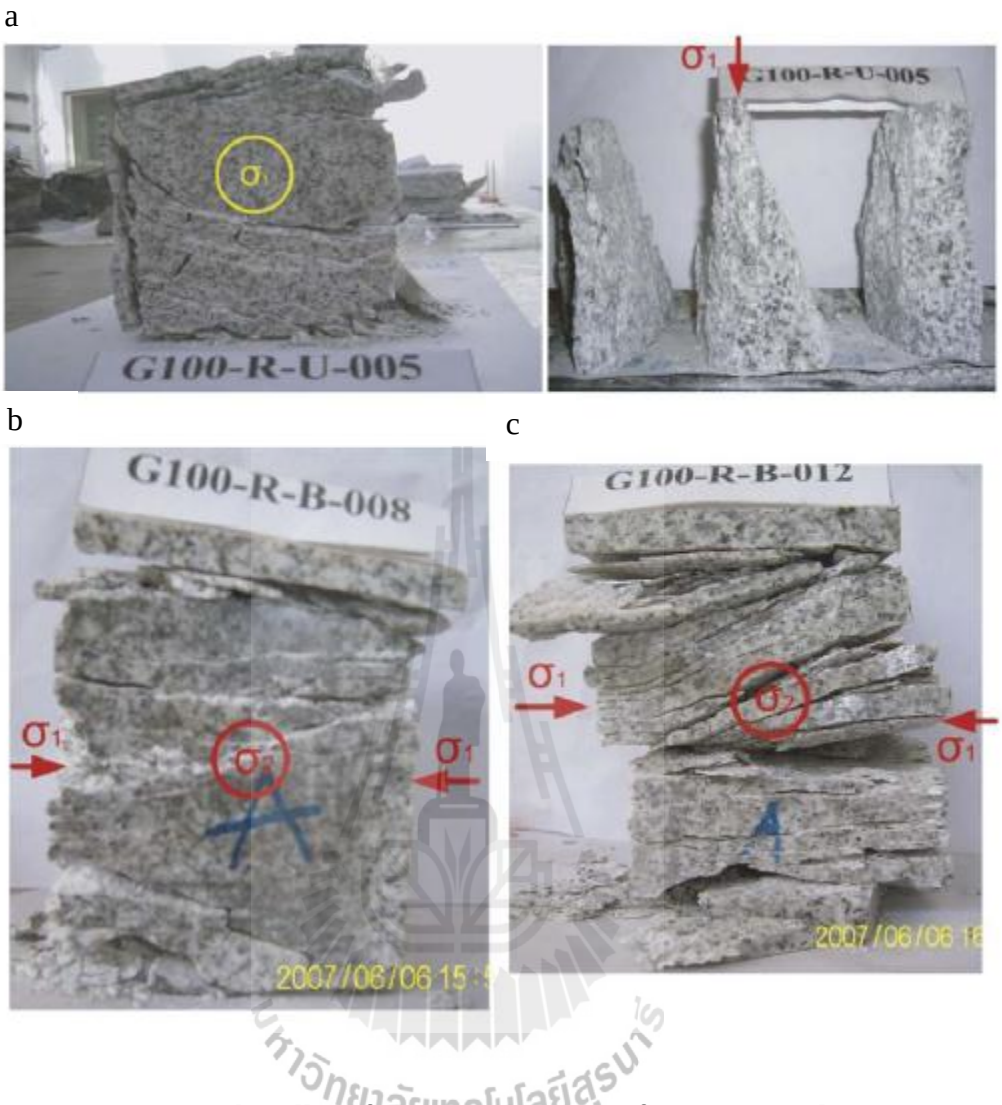

Figure 2.13 Typical spalling failure mechanisms of granite samples: (a) uniaxial; (b) biaxial-loading path 1; (c) biaxial-loading path 2 – more spalling is observed under higher confinement (Yun et al, 2010).

changes the mechanical and hydraulic properties of the rock mass. The test rock models have a persistent joint set with dip angles of 30°, 45° and 60° to the horizontal. Under the applied biaxial compression, tension crack initiation and propagation are the dominant fracture behaviors around the hole in a low joint dip angle rock model (30° to the horizontal). The propagation direction of the tensile

cracks is roughly normal to the joint surface, and with propagation of tensile cracks, removable rock block are generated. The experimental results are simulated using discrete element code. The numerical analysis simulates several aspects of rock mass cracking and the joint sliding processes around an opening: progressive fracture behaviors in a low joint angle rock model, abrupt initiation and propagation of tensile cracks and joint sliding in a high joint angle rock model (60° to the horizontal), propagation of tensile cracks normal to the joint surface, generation of removable blocks in rock segments, an increase of lower hoop stress threshold inducing tensile fractures with a decrease in the joint rock angle, and an increase of the damage zone around the hole with a decrease in the joint angle.

CHAPTER III

DESIGN AND FABRICATION OF UNIAXIAL-TO-BIAXIAL LOAD CONVERTER

3.1 Introduction

The UBC has been developed for using to test rock specimens under true biaxial stress state. The UBC has been designed Solidworks program. The factor of safety is calculated. The frame performance is assessed by conducting biaxial compression tests to study the deformation and failure characteristics of rock specimens. This chapter describes the design requirements and components of the UBC and calculations of the factor of safety.

3.2 Design requirements and components

The device is made of hard steel, as shown in Figure 3.1. The UBC is developed based on the three design requirements: (1) capable of maintaining constant lateral stresses during the test, (2) design and invention of the new device is compatible with most compression load frame and (3) allowing monitoring deformation displacement of the specimen during the experiment. To meet the load requirement above, two pairs of loading platens are used to apply the lateral stresses in mutually perpendicular directions to the rock specimen. The force diagram is shown in Figure 3.2. The load frame is applied by a 750 kN hydraulic load cell.

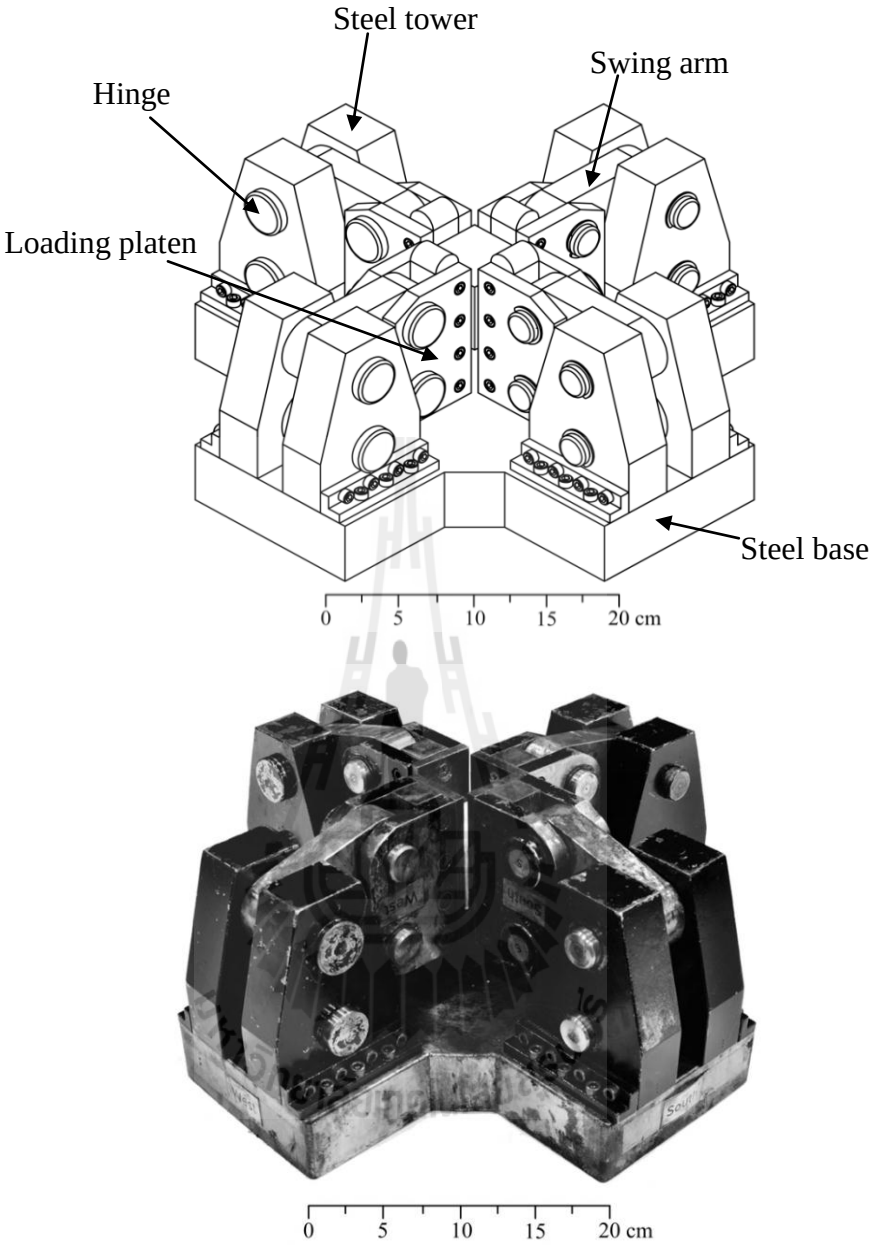

Figure 3.1 The uniaxial-to-biaxial load converter (UBC) and its components.

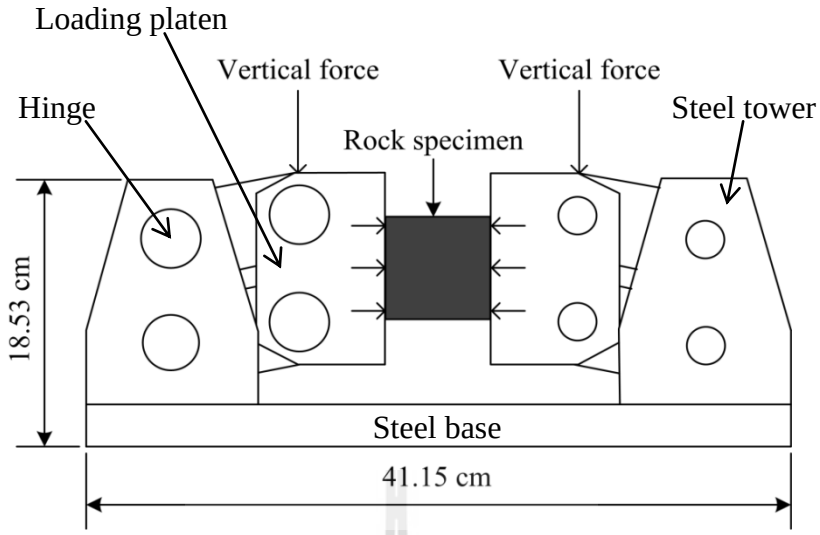

Figure 3.2 UBC load cantilever from vertical to horizontal direction.

The UBC can accommodate specimen sizes from 25×25×25 mm^3 up to 65×65×100 mm^3. The different specimen sizes and shapes can be tested by adjusting the distances between the opposite loading platens. Figure 3.3 shows the UBC's top view. The lateral loads are obtained by two sets of swing arms arranged in mutually perpendicular directions. The outer ends of these swing arms are hinged on steel towers. The inner ends are securely attached to load steel platens. The vertical loads can be applied on the platens simply by using a uni-directional load frame. The UBC comprises steel base, hinges, swing arms, steel towers and loading platens. The base is 50.8 mm thick and 411.5 mm long. The thickness of swing arm is 25.4 mm and 126.8 mm long. The height trapezoid steel tower is 134.5 mm. The area of loading platen is 645.12 mm^2. Figure 3.4 through Figure 3.12 show the dimensions of each component of UBC.

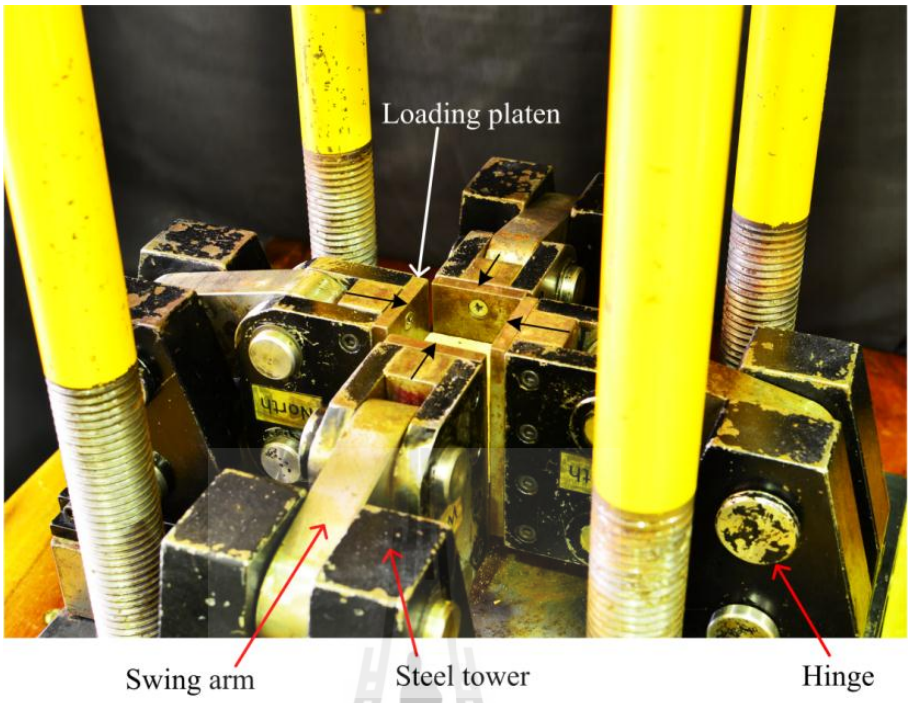

Figure 3.3 UBC placed in a conventional uniaxial load frame.

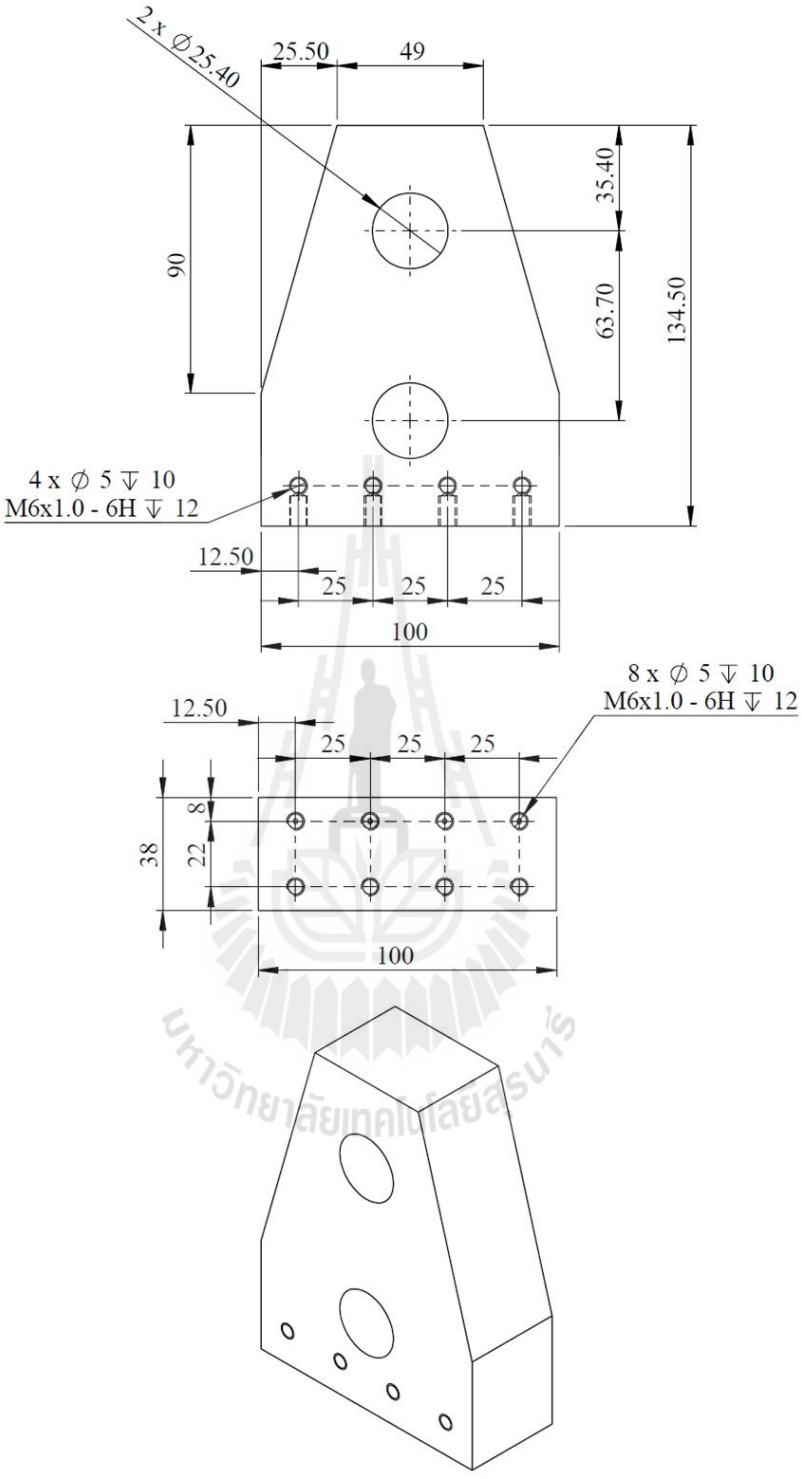

Figure 3.4 Dimensions of steel tower in millimeter scale.

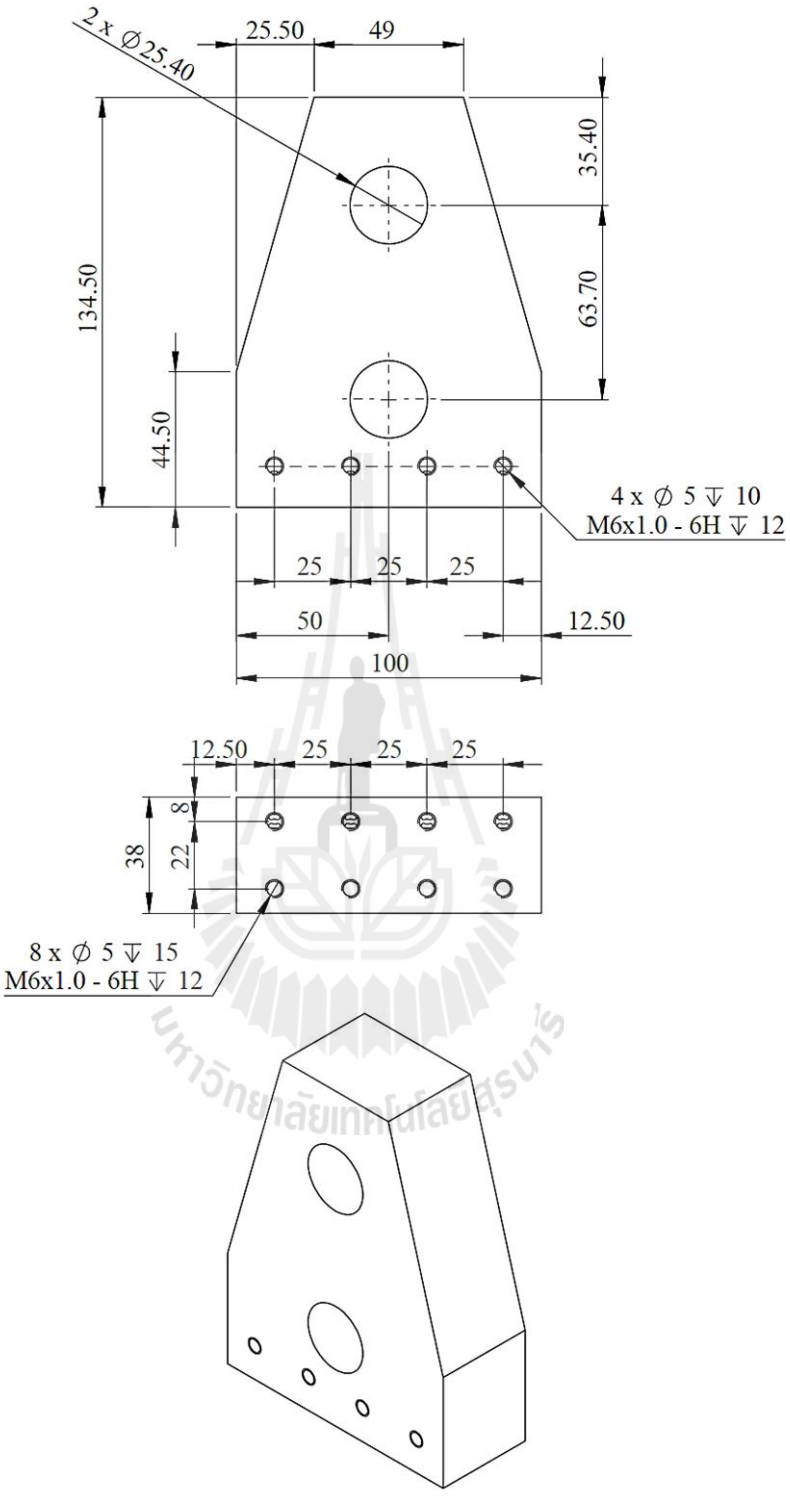

Figure 3.5 Dimensions of steel tower (cont.) in millimeter scale.

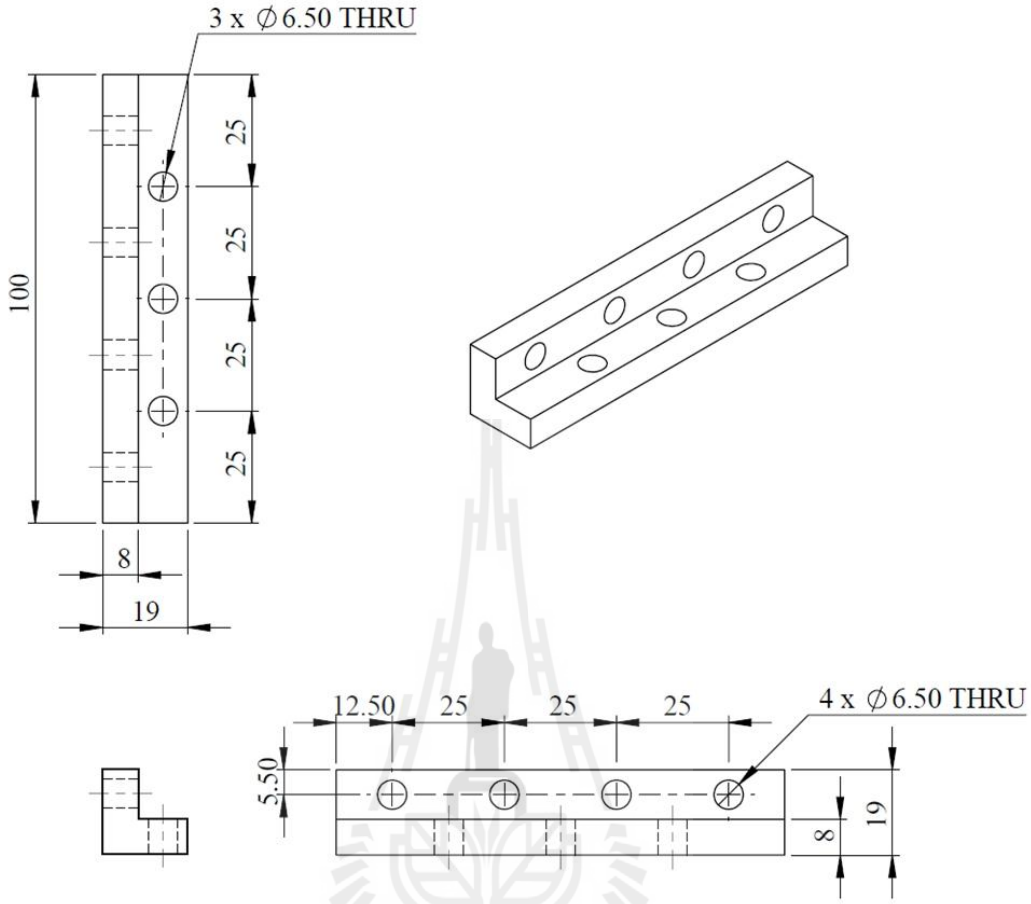

Figure 3.6 Details of L-shaped steel plate in millimeter scale.

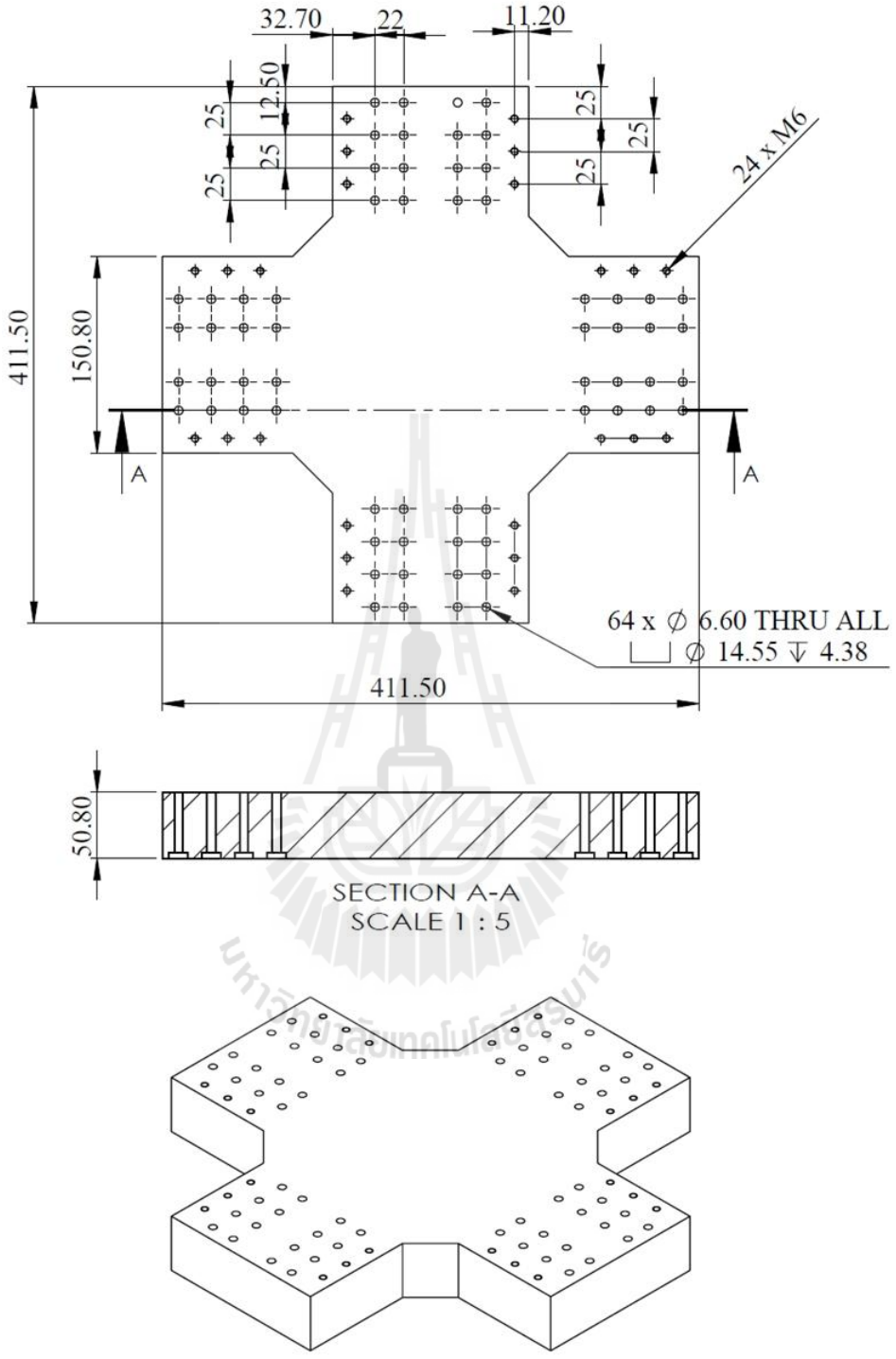

Figure 3.7 Dimensions of steel base in millimeter scale.

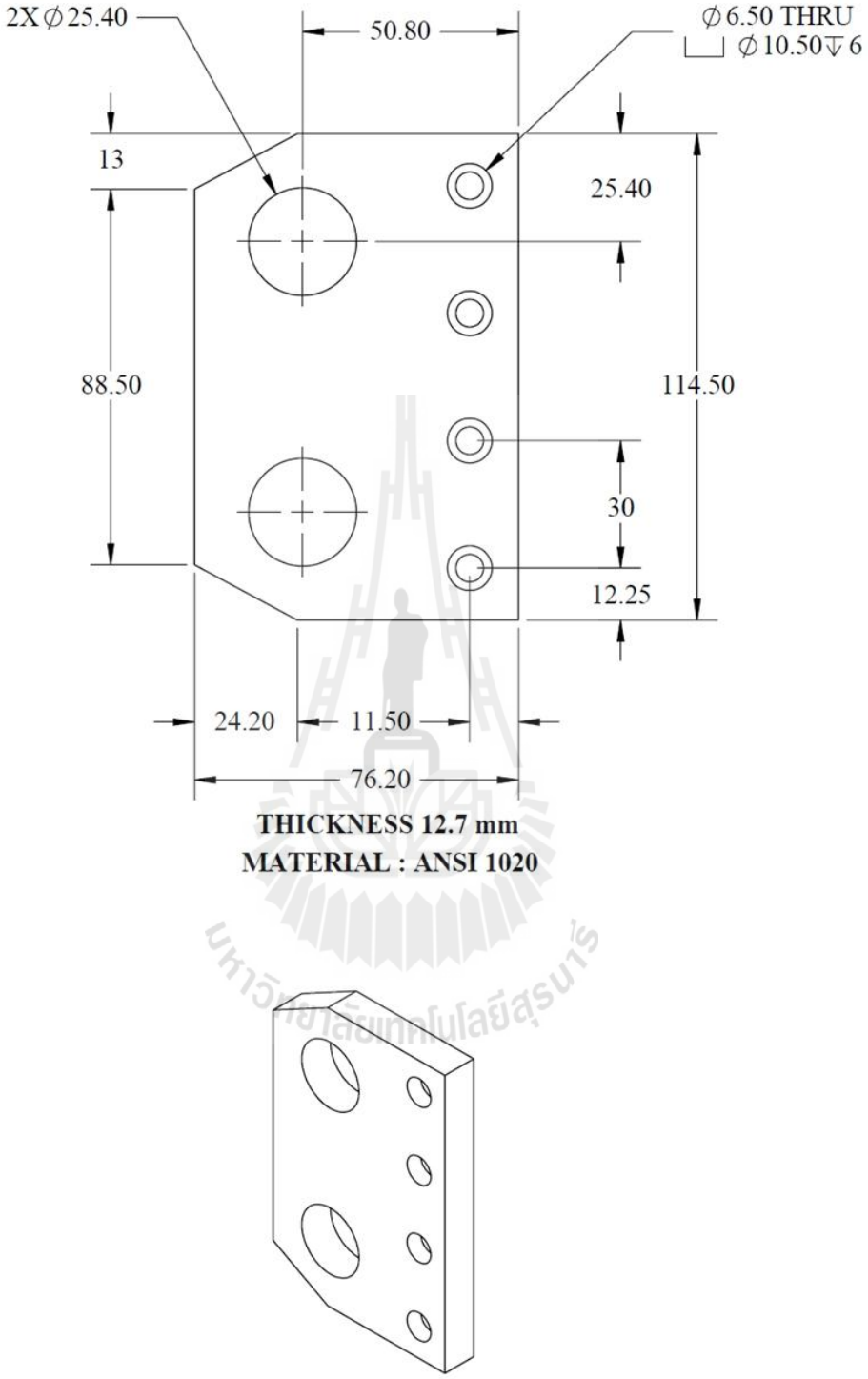

Figure 3.8 Dimensions of loading platen in millimeter scale.

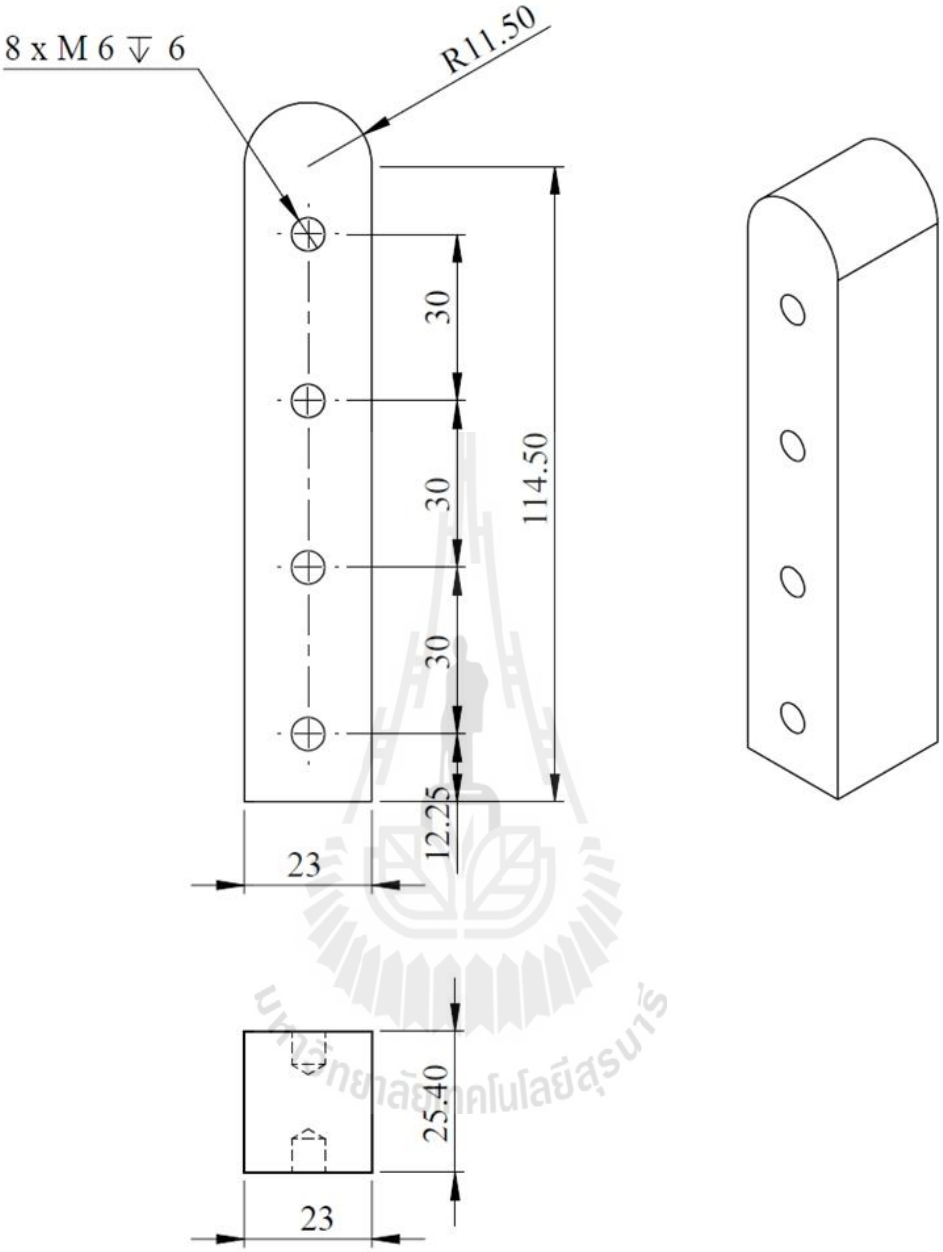

Figure 3.9 Dimensions of middle steel of loading platen in millimeter scale.

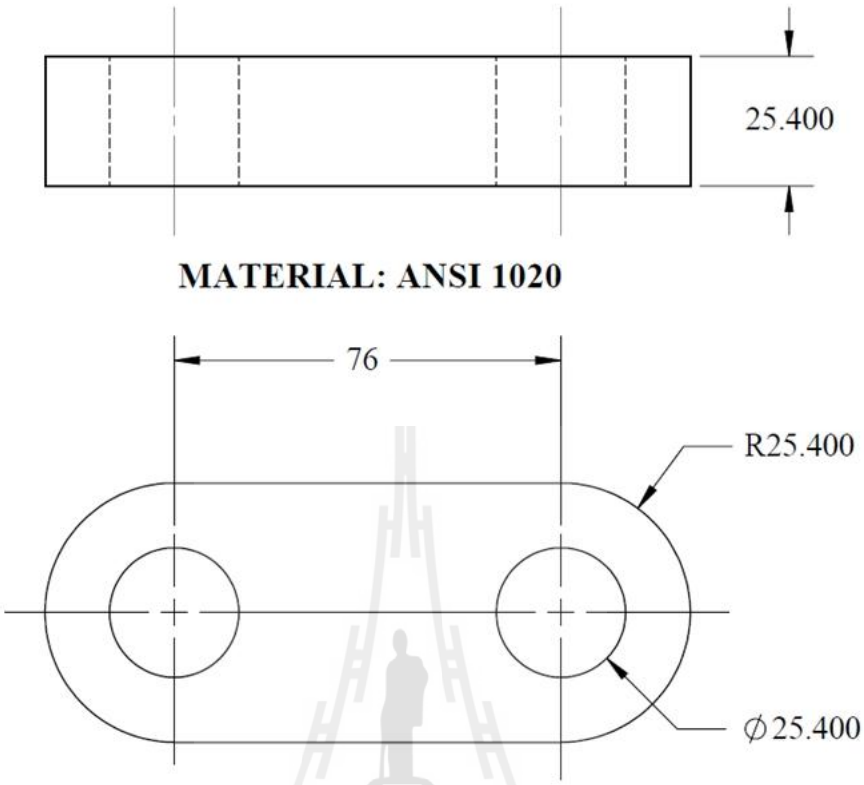

Figure 3.10 Dimensions of swing arm in millimeter scale.

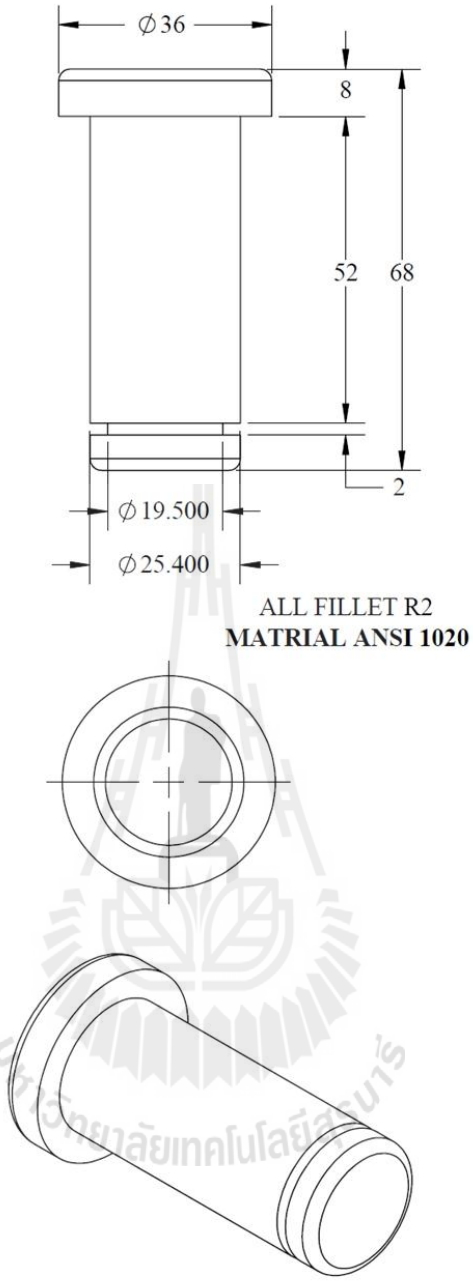

Figure 3.11 Dimensions of steel hinge (1) in millimeter scale.

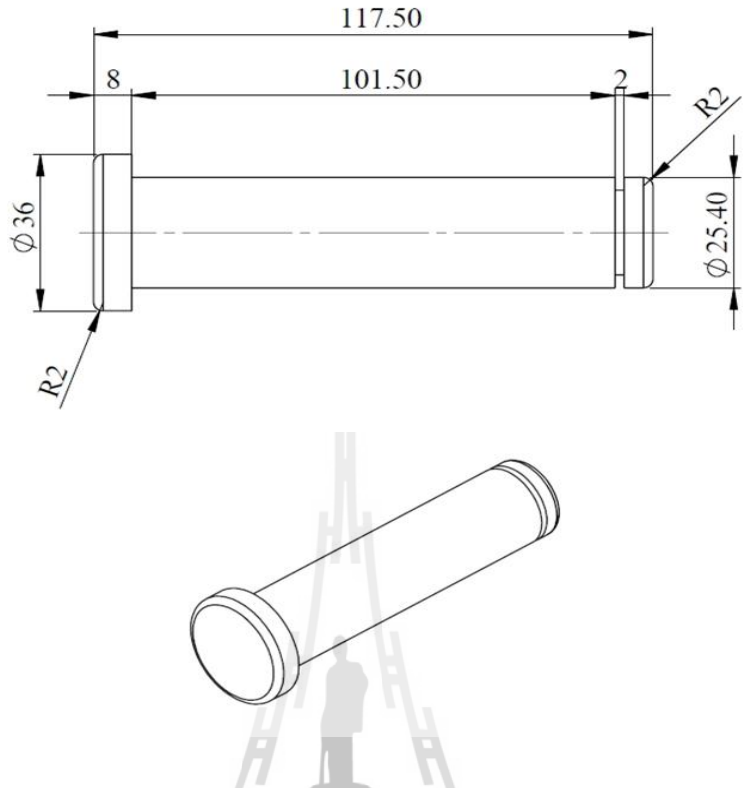

Figure 3.12 Dimensions of steel hinge (2) in millimeter scale.

3.3 Calculations of factor of safety

The UBC is made of structural steel A36 (SS400). The mechanical properties of the material are shown in Table 3.1.

3.3.1 Factor of safety of swing arms (in bending)

The factor of safety of swing arms in bending is calculated by (Hibbeler, 2008):

$$\sigma_{max} = \frac{Mc}{I} \tag{3.1}$$

where σ_{max} is the maximum normal stress in the member, M is the internal moment, I is the moment of inertia of the cross-section area and c is the perpendicular distance from the neutral axis to a point farthest away from the neutral axis, where σ_{max} acts.

The factor of safety of swing arms in bending condition is calculated by using equation (3.1). The maximum internal moment in swing arms is 1947.332 N.m, the moment of inertia is 2.775×10^{-7} m^4, perpendicular distance is 0.0254 m and yielding strength of steel is 250 MPa. The factor of safety is 1.403.

3.3.2 Factor of safety of swing arms (in compression)

The factor of safety of swing arms in compression stress condition is calculated by (Hibbeler, 2008):

$$P_{cr} = \frac{\pi^2 EI}{L^2} \tag{3.2}$$

where P_{cr} is critical load capacity of swing arms, E is modulus of elasticity of steel, I is the moment of inertia of the cross-section area and L is length of column.

Table 3.1 Mechanical properties of structural steel A36 (SS400) (Hibbeler, 2008).

Density (kg/m^3)	Poisson's Ratio (ν)	Modulus of Elasticity (GPa)	Modulus of Rigidity (GPa)	Yield Strength (MPa)		Ultimate Strength (MPa)	
				Tension	Compression	Tension	Compression
7860	0.32	200	75	250	250	400	400

The factor of safety of swing arms in compression is calculated by using equation (3.2). The maximum axial load used is 21,932.796 kN per arm. The modulus of elasticity of beam is 200 GPa, the moment of inertia is 2.775×10^{-7} m^4 yielding strength of steel is 250 MPa and length of beam is 0.1268 m. The critical axial load on the column just before it begins to buckle is 34,068.595 kN. The factor of safety for swing arms in compression stress is calculated as 1.553.

3.3.2 Factor of safety of hinge

The factor of safety of hinge under shear stress condition is calculated by: (Hibbeler, 2008)

$$\tau_{max} = 4V/3A \tag{3.3}$$

where τ_{max} is maximum shear stress in the hinge, A is cross-sectional area of the hinge, V is shear force and the largest shear stress in a hinge is about 4/3 times the average shear stress.

The factor of safety of hinges in shear stress is calculated by using equation (3.3). The ultimate shear strength is 220 MPa. The maximum shear stress in hinge is 70.455 MPa. The shear force is 26,775 kN. The cross-sectional area of the hinge is 5.067×10^{-4} m^2. The factor of safety for the hinge in shear stress is calculated as 3.123.

CHAPTER IV

TEST METHOD OF THE UBC

4.1 Introduction

This chapter describes the UBC load calculation, load calibration and test procedure. The results of the calibration will be used to determine the failure load for the biaxial compressive strength testing.

4.2 Theoretical load calculation

The calculation of UBC loads for one lateral loading direction assumes that its components are rigid (Hibbeler, 2010). The horizontal load is calculated using the free-body diagram as shown in Figure 4.1. The horizontal load is calculated from the applied vertical load. The optimum angle of the swing arm is set at 35°. The calculation result for the static equilibrium force indicates that $F_h = 1.4F_v$, or the horizontal force (F_h) is about 70% of the vertical force (F_v), as shown in Figure 4.2.

4.3 Actual load calibration

The actual lateral load is calibrated using an electronic load cell, as shown in Figure 4.3. The calibration load is measured from the strains included on the surfaces of a cubical steel block while under uniaxial and biaxial loadings. The calibrated strains for the uniaxial compression and biaxial compression are obtained from strain gages attached on the cubical shaped steel block (Figure 4.4). The vertical load on UBC can be obtained from any conventional uniaxial load frame equipped with a

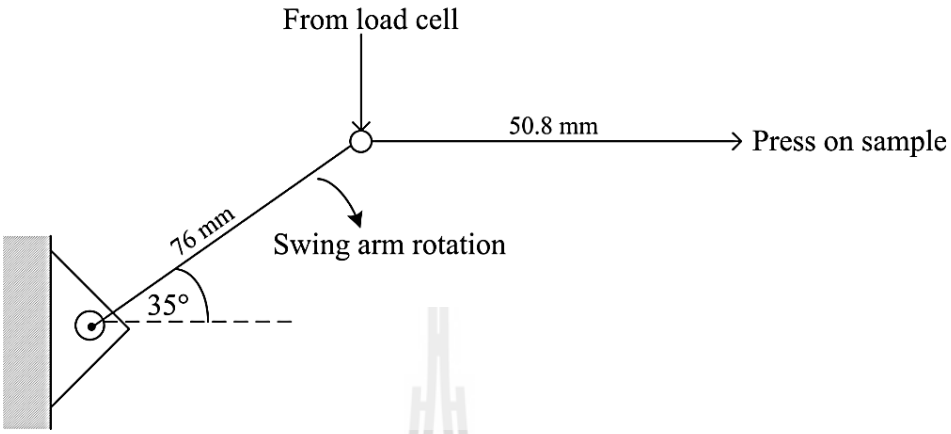

Figure 4.1 Free-body diagram (FBD) used for the force calculation.

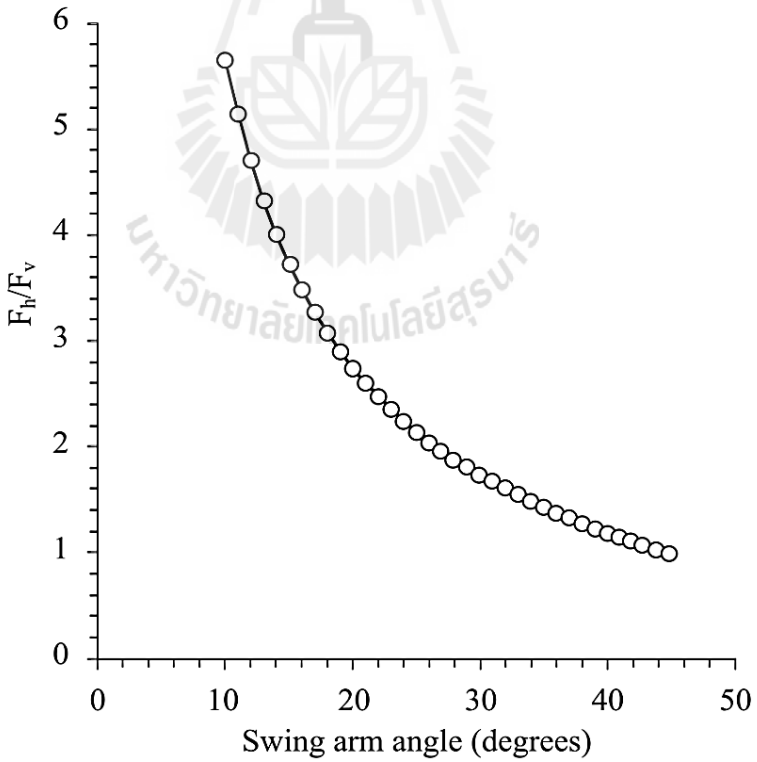

Figure 4.2 Horizontal-to-vertical force ratio as a function of swing arm rotation.

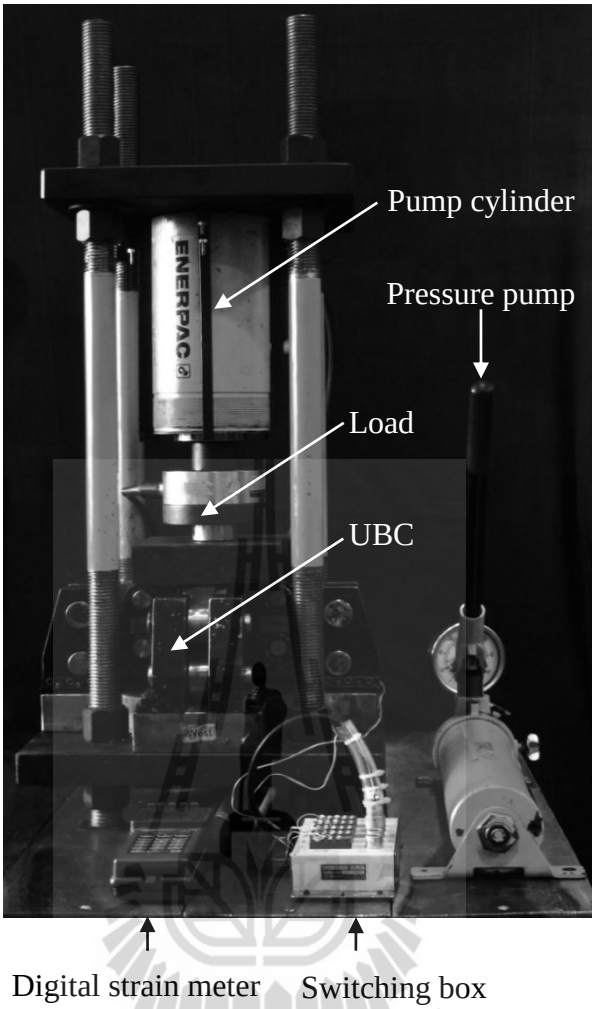

Figure 4.3 UBC arranged in uniaxial load frame during calibration.

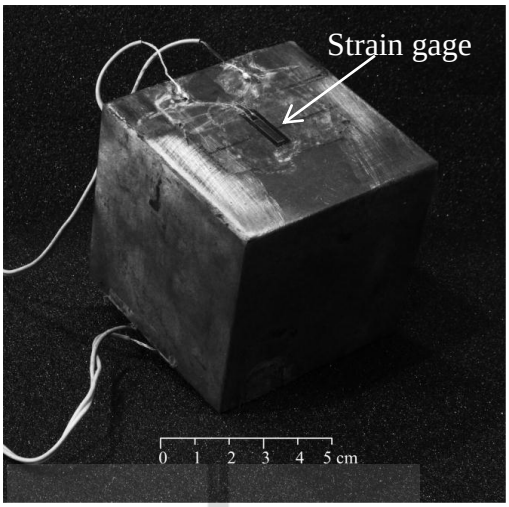

Figure 4.4 Steel block attached with strain gages used for the calibration.

hydraulic load cell. Calibration curves are developed to correlate the applied vertical load with the lateral loads by using a high precision electronic load cell and a reference cubical steel block attached with two directional strain gages. The calibration results are used to determine the lateral stresses applied on the specimen while the vertical load is increased. The vertical displacement of the swing arms at the point where the vertical load is applied is also calibrated with the lateral movement of the four loading platens.

The vertical to horizontal displacement ratio (d_v/d_h) is used to determine the lateral deformation of the specimen by monitoring the vertical movement of the loading platens, as shown in Figure 4.5. The maximum lateral load is designed for 150 kN. The axial load is applied by a hydraulic load cell with maximum capacity of 75 MPa. The UBC can accommodate specimen sizes from 25×25×25 mm^3 to 65×65×100 mm^3. Figure 4.6 compares the calibration curve between the uniaxial force applied on UBC and the uniaxial force applied by a load frame via strain gages

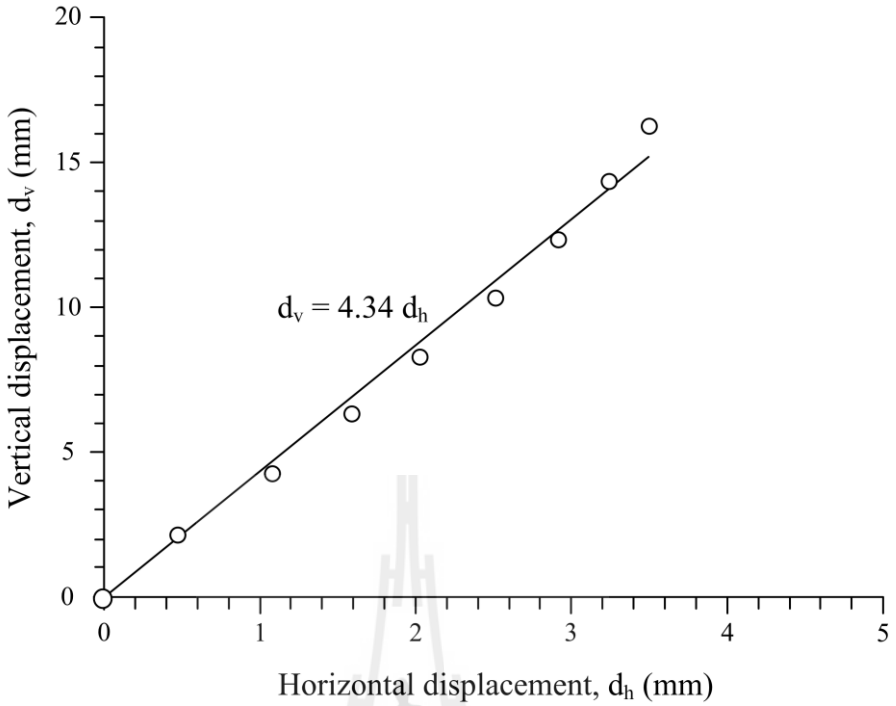

Figure 4.5 Vertical displacement as a function of lateral displacement.

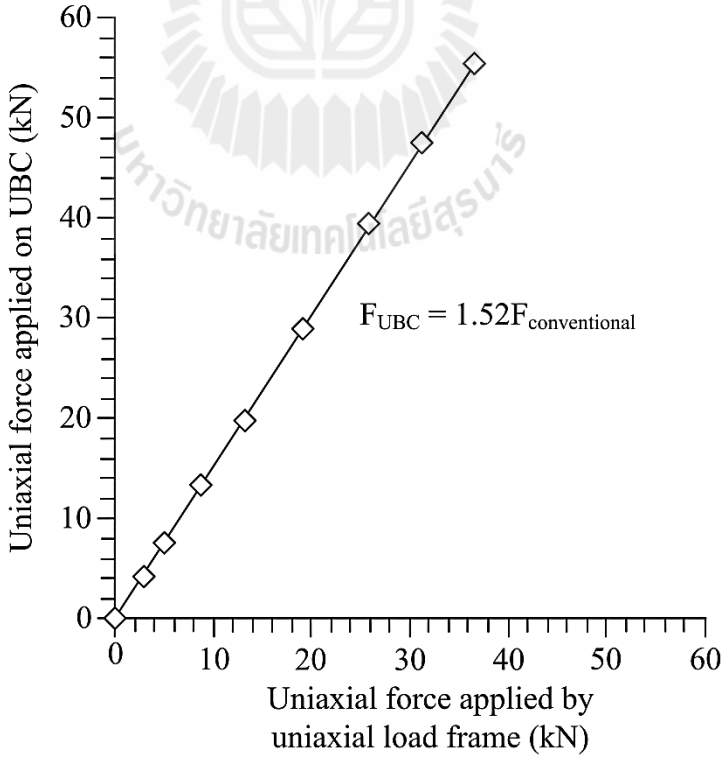

Figure 4.6 Calibration of the UBC force by comparing with a uniaxial load frame.

and electronic load cell. Figure 4.7 compares the calibration curves between biaxial force applied on UBC and the force applied by a biaxial load frame. There curves will be used to determine the lateral stress of UBC on the specimen.

4.4 Test procedure

The rock specimen prepared with nominal dimensions of 50×50×50 mm^3 is recommended. The test procedure comprising (1) specimen installation and (2) uniaxial and biaxial compressive strength testing.

4.4.1 The specimen installation

- insert neoprene sheets on four sides of rock specimens
- install the prepared specimen in the center of the UBC
- adjust the swing arms to attach the specimen on two sides for uniaxial testing and four sides for biaxial testing
- ensure that the loading platens are in contact with the specimen and are in the horizontal position, as shown in Figure 4.8

4.4.2 The uniaxial and biaxial compressive strength test procedure

- place the UBC in a uniaxial load frame
- insert the neoprene sheet between the top platen of the UBC and square steel plate to reduce the friction
- place a load cell with a precision of ±0.01 kN, and attach the deformation dial gages on four sides
- increase the vertical load using the hydraulic pressure cell
- record the readings from the dial gages and pressure gage
- increase the load until failure occurs

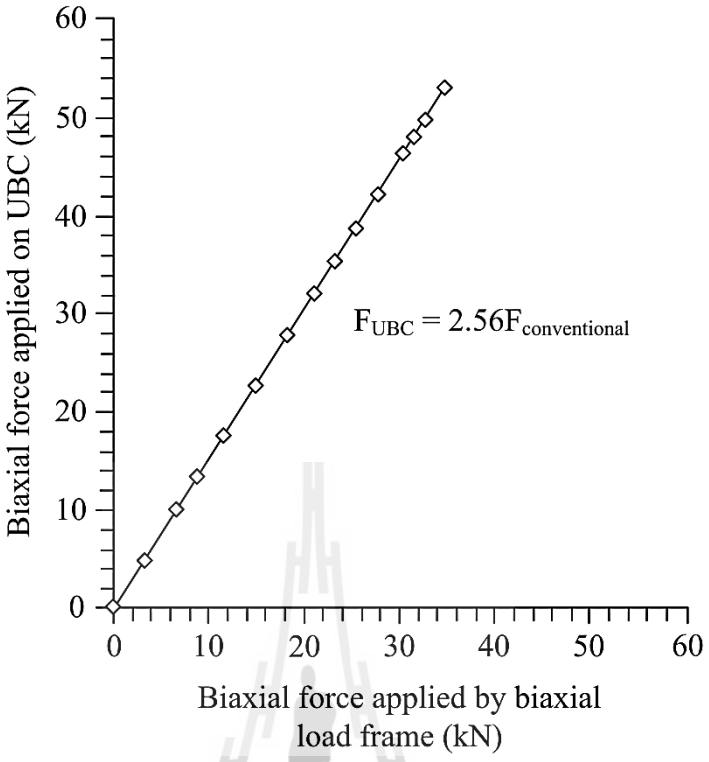

Figure 4.7 Calibration force of UBC from biaxial load frame.

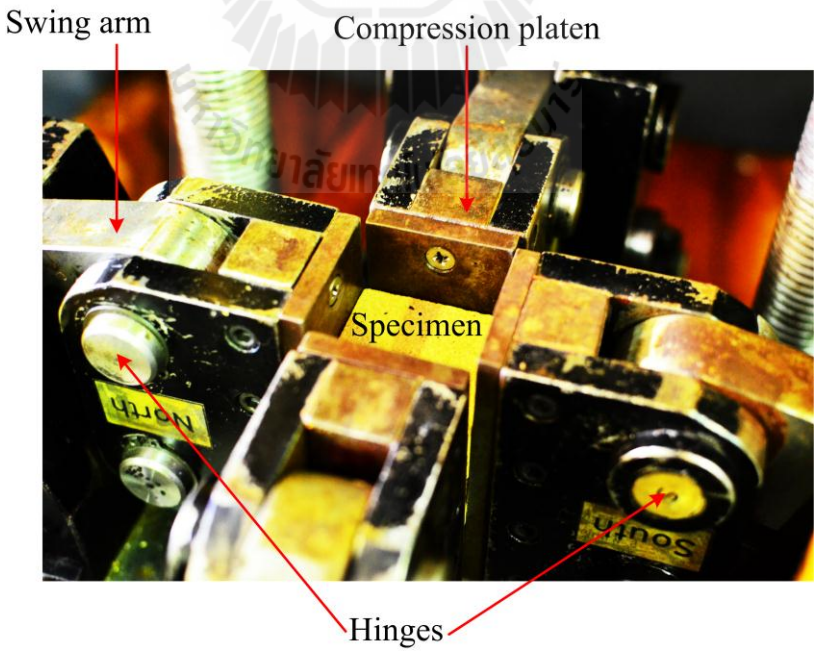

Figure 4.8 Close-up picture of specimen between four lateral loading platens**.**

CHAPTER V

SAMPLE PREPARATION

5.1 Introduction

This chapter describes sample preparation and specifications of the tested specimen. Sample preparation has been carried out in the Geomechanics laboratory at the Suranaree University of Technology.

5.2 Test specimens

Phra Wihan sandstone, Phu Phan sandstone, Phu Kradung sandstone, Saraburi marble and Maha Sarakham salt (hereafter designated as PW, PP, PK, SM and MS) have been selected and prepared to obtain cubic-shaped specimens, as shown in Figure 5.1.

The test sandstones belong to the Khorat group which widely expose in the north and northeast of Thailand. Petrographic analyses have been performed by Thosuwan (2009) to determine their mineral compositions. Table 5.1 summarizes the results. The tested sandstones are classified as fine-grained quartz sandstones. There rocks are selected primarily because of their highly uniform texture, grain size and density. The average grain size of the sandstone is 0.1-1.0 mm.

SM is collected from Saraburi province, Thailand. It is 100% calcite with average grain size of 1-5 mm, as given by Kemthong and Fuenkajorn (2007).

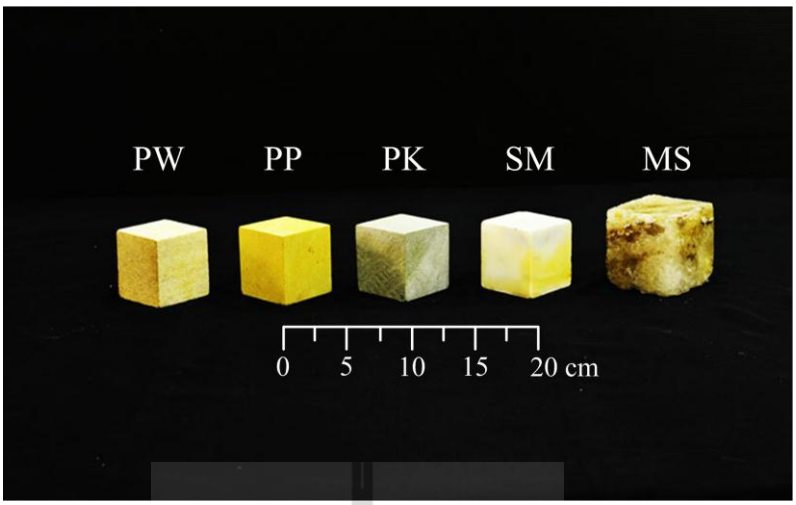

Figure 5.1 Some pre-test specimens for five rock types.

Table 5.1 Mineral compositions of tested sandstones obtained by Petrographic analyses (Thosuwan, 2009).

Rock Name	Density (g/cc)	Color	Compositions				
			Quartz (%)	Albite (%)	Kaolinite (%)	Feldspar (%)	Mica (%)
PW sandstone	2.35	white	99.47	-	0.53	-	-
PP sandstone	2.45	yellow	98.40	-	-	-	1.60
PK sandstone	2.63	green	48.80	46.10	5.10	-	-

MS is the middle members of the Maha Sarakham formation in the Khorat basin, northeastern Thailand. The rock salt is relatively pure halite with a slight amount (less than 1-2%) of anhydrite, clay minerals and ferrous oxide. The average crystal (grain) size is about 5×5×10 mm^3, as given by Sriapai 2010.

5.3 Specimen sizes

The test specimens have been cut to obtain cubic-shape using a tile cutter (Model ZE-LG3-570A), as shown in Figure 5.2. The sandstones and SM have been prepared with nominal dimensions of 50×50×50 mm^3. MS is dry cut by cutting machine (Figure 5.3) with nominal dimensions of 54×54×54 mm^3. Tables 5.2 through 5.6 summarize the specimen, dimensions and density. The dimensions of test specimens are measured using a caliper to the nearest 0.25 mm at the centers of the end faces.

Figure 5.2 Tile cutter used to prepare sandstone specimens.

Figure 5.3 MS is dry cut by a cutting machine.

Table 5.2 Dimensions and density of PW sandstone.

Specimen no.	Width (mm)	Length (mm)	Height (mm)	Density (g/cc)
PW-UCS-01	52.30	50.30	51.30	2.17
PW-UCS-02	50.45	49.50	51.30	2.19
PW-UCS-03	50.40	51.60	49.50	2.23
PW-UCS-04	51.20	49.70	50.45	2.23
PW-UCS-05	50.50	51.10	51.30	2.21
PW-UCS-06	50.40	51.45	49.50	2.22
PW-UCS-07	52.75	50.40	51.45	2.26
PW-UCS-08	50.95	52.40	50.40	2.25
PW-UCS-09	50.85	51.10	51.30	2.20
PW-UCS-10	49.40	50.70	50.90	2.22
PW-BI-01	49.79	50.50	51.58	2.26
PW-BI-02	50.67	50.22	50.80	2.31
PW-BI-03	50.45	49.20	50.60	2.23
PW-BI-04	50.50	51.48	51.28	2.23
PW-BI-05	50.35	50.40	103.5	2.25
PW-BI-06	50.40	50.20	103.1	2.23

Table 5.3 Dimensions and density of PP sandstone.

Specimen no.	Width (mm)	Length (mm)	Height (mm)	Density (g/cc)
PP-UCS-01	51.10	51.05	50.80	2.42
PP-UCS-02	51.25	51.45	49.50	2.40
PP-UCS-03	50.35	51.10	51.40	2.39
PP-UCS-04	51.40	49.85	50.80	2.41
PP-UCS-05	51.90	51.60	51.00	2.41
PP-UCS-06	51.40	51.45	49.50	2.45
PP-UCS-07	52.05	50.40	50.25	2.44
PP-UCS-08	50.70	50.25	50.15	2.43
PP-UCS-09	50.85	51.10	51.30	2.40
PP-UCS-10	49.40	50.70	50.90	2.42
PP-BI-01	49.00	50.65	51.00	2.39
PP-BI-02	50.37	49.50	51.12	2.38
PP-BI-03	50.30	51.00	50.80	2.42
PP-BI-04	50.45	50.08	50.45	2.40
PP-BI-05	50.08	50.80	51.08	2.39
PP-BI-06	50.01	49.92	49.92	2.36

Table 5.4 Dimensions and density of PK sandstone.

Specimen no.	Width (mm)	Length (mm)	Height (mm)	Density (g/cc)
PK-UCS-01	50.00	50.95	50.80	2.51
PK-UCS-02	50.50	50.75	51.45	2.54
PK-UCS-03	50.15	51.40	50.80	2.50
PK-UCS-04	50.12	50.30	49.82	2.53
PK-UCS-05	51.28	51.10	48.74	2.56
PK-UCS-06	51.00	51.15	49.50	2.54
PK-UCS-07	50.70	50.68	50.25	2.53
PK-UCS-08	50.00	51.30	50.15	2.56
PK-UCS-09	51.40	49.85	50.80	2.50
PK-UCS-10	51.90	51.60	51.00	2.52
PK-BI-01	50.89	51.20	50.50	2.51
PK-BI-02	50.37	49.92	51.58	2.54
PK-BI-03	50.30	48.44	51.00	2.55
PK-BI-04	51.48	48.00	51.48	2.50
PK-BI-05	50.59	51.40	51.28	2.51
PK-BI-06	49.64	50.30	51.10	2.53

Table 5.5 Dimensions and density of Saraburi marble.

Specimen no.	Width (mm)	Length (mm)	Height (mm)	Density (g/cc)
SM-UCS-01	50.40	54.54	49.50	2.65
SM -UCS-02	51.80	50.42	51.15	2.66
SM -UCS-03	50.00	49.62	50.68	2.67
SM -UCS-04	50.40	51.45	49.50	2.66
SM -UCS-05	52.75	50.40	51.45	2.65
SM -UCS-06	50.95	52.40	50.40	2.65
SM -UCS-07	50.85	51.10	51.30	2.66
SM -UCS-08	49.40	50.70	50.90	2.67
SM -UCS-09	51.00	51.45	51.30	2.65
SM -UCS-10	50.70	50.70	50.15	2.66
SM -BI-01	50.54	50.10	51.30	2.67
SM -BI-02	49.00	50.00	51.58	2.67
SM -BI-03	51.39	48.44	50.50	2.65
SM -BI-04	50.89	51.20	50.50	2.66
SM -BI-05	51.73	49.92	51.58	2.65
SM -BI-06	50.65	48.44	51.00	2.67

Table 5.6 Dimensions and density of Maha Sarakham salt.

Specimen no.	Width (mm)	Length (mm)	Height (mm)	Density (g/cc)
MS-UCS-01	56.50	57.80	54.31	2.14
MS -UCS-02	54.30	53.85	54.34	2.24
MS -UCS-03	55.50	57.00	54.20	2.26
MS -UCS-04	54.30	54.30	54.30	2.24
MS -UCS-05	54.45	55.50	55.30	2.19
MS -UCS-06	55.20	54.60	55.50	2.32
MS -UCS-07	54.50	54.70	54.45	2.19
MS -UCS-08	55.10	55.10	55.30	2.18
MS -UCS-09	54.25	56.05	54.80	2.28
MS -UCS-10	54.35	54.45	55.35	2.19
MS -BI-01	54.05	57.00	54.48	2.25
MS -BI-02	55.60	55.10	54.26	2.29
MS -BI-03	55.25	57.20	54.80	2.30
MS -BI-04	54.40	54.65	54.58	2.20
MS -BI-05	56.18	55.40	54.50	2.22
MS -BI-06	57.25	56.30	55.10	2.00

CHAPTER VI

TEST RESULTS

6.1 Introduction

The objective of the laboratory tasting is to assess the performance of the UBC. The results are compared with those of the conventional biaxial load frame. This chapter describes the test results. The tasks include the uniaxial compressive strength test using conventional frame, uniaxial compression test using UBC, biaxial compressive strength test using conventional frame and biaxial compression test using UBC.

6.2 Laboratory tests

The objective of the tests is to develop a data basis to compare with the conventional biaxial compression test results. The cube-shaped specimens are tested in laboratory to simulate the effects of the confining pressures at the underground opening boundaries.

6.2.1 Uniaxial compression strength test using conventional frame

The unconfined compressive strength of the rock specimens is performed in accordance with the ASTM standard practice (ASTM D7012-04) and the suggested method of the ISRM (Brown, 1981). A uniform axial load is applied to the cubical block rock specimens at a constant rate of 0.5-1 MPa/second until failure. The axial displacements are monitored by displacement dial gages with a precision of 0.01

mm. The conventional uniaxial compressive strengths for the PW, PP, PK, SM and MS are 23.4±1.2, 32.3±1.9, 31.8±2.2, 22 and 21.9±1.9 MPa, respectively. The test results are plotted in Figures 6.1. The elastic moduli are 11.3, 11.4, 10.3, 25.1 and 21.6 GPa.

6.2.2 Uniaxial compression test using UBC

The uniaxial compressive strengths of five rock types are determined by using UBC. The uniaxial compressive strengths obtained from the UBC for the PW, PP, PK, SM and MS are 21.1±1.5, 33.4±1.5, 30.7±0.5, 24.7±1.1 and 21.7±0.9 MPa, respectively. The stress-strain curves are plotted in Figure 6.2. The elastic moduli are 11.9, 11.5, 10.4, 25.5 and 20.7 GPa.

6.2.3 Biaxial compression test using conventional frame

The biaxial compression tests are performed by using conventional biaxial load frame. The maximum principal stress (σ_1) is equal to the intermediate principal stress (σ_2). The stresses are increased until failure occurs. The measured deformations are used to determine the strain along the principal axes during loading. The failure stresses are recorded and mode of failure is examined. The biaxial compressive strengths of PW, PP, PK, SM and MS are 39, 59 ± 1.4, 57.7 ± 1.2, 34 and 37.9 ± 0.6 MPa, respectively. The test results are plotted in Figures 6.3. The elastic moduli are 11.7, 11.2, 11.9, 25.0 and 20.3 GPa.

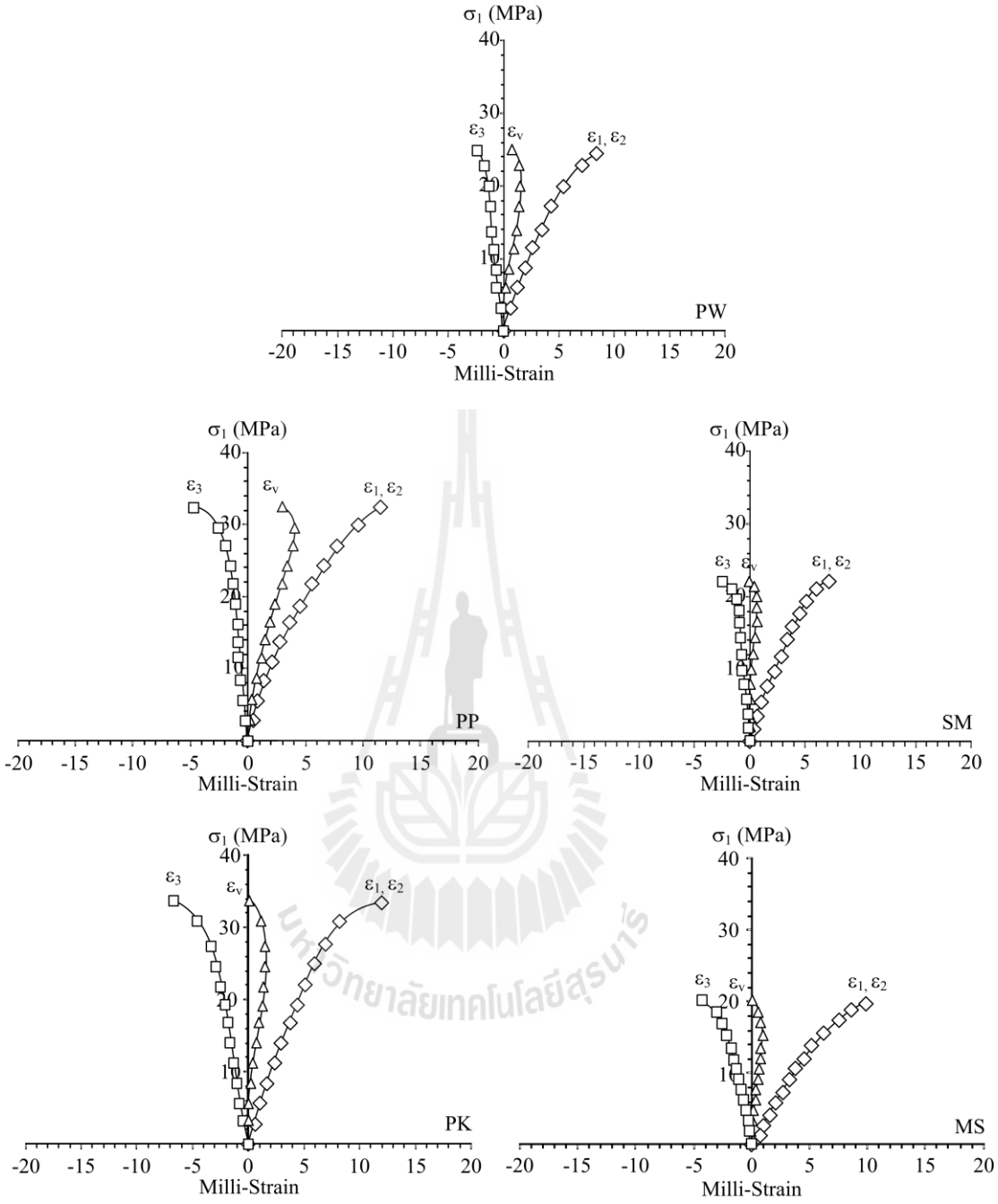

Figure 6.1 Stress-strain curves from uniaxial compressive strength test using conventional load frame.

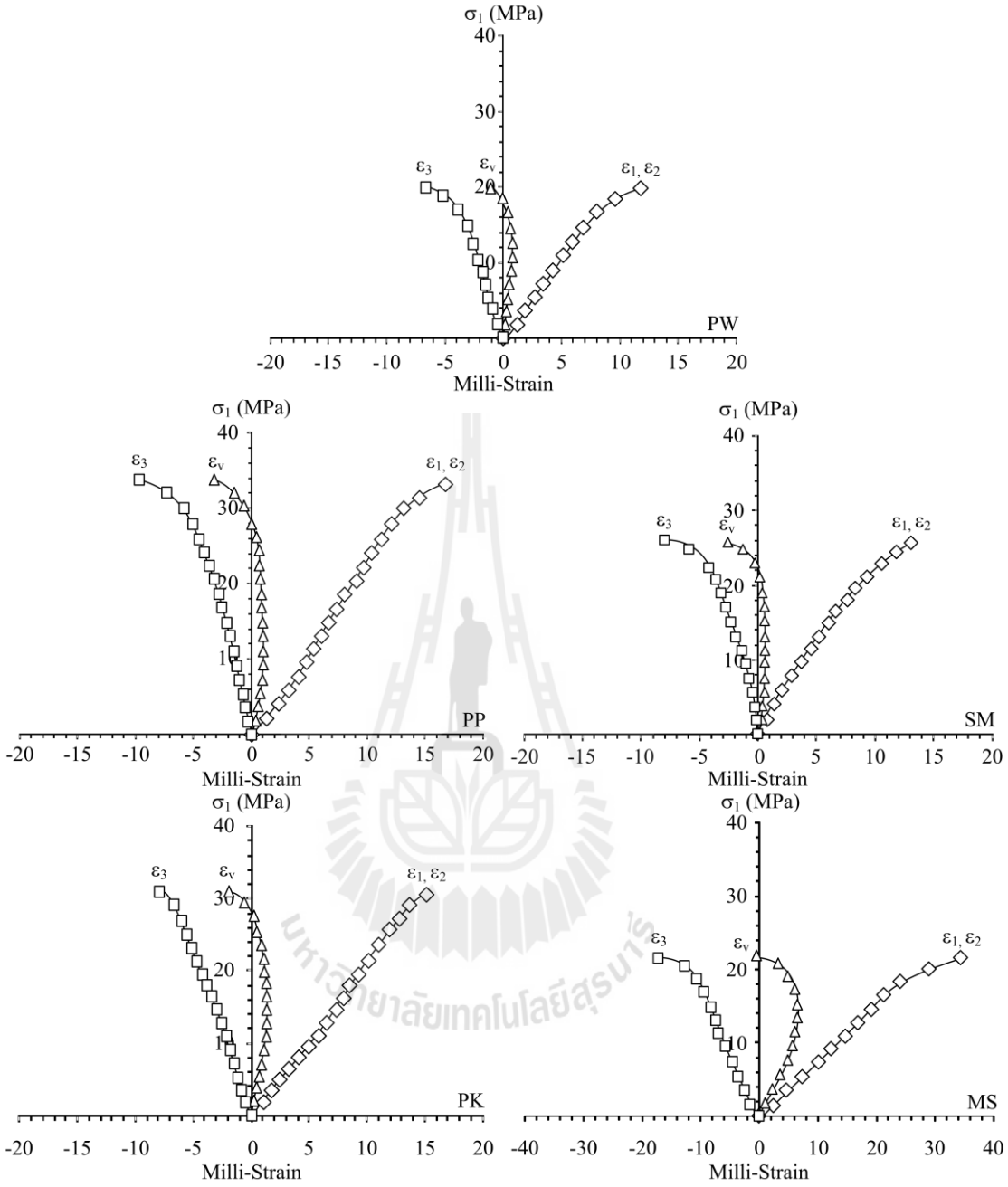

Figure 6.2 Stress-strain curves of five rock types from uniaxial compressive strength test using UBC.

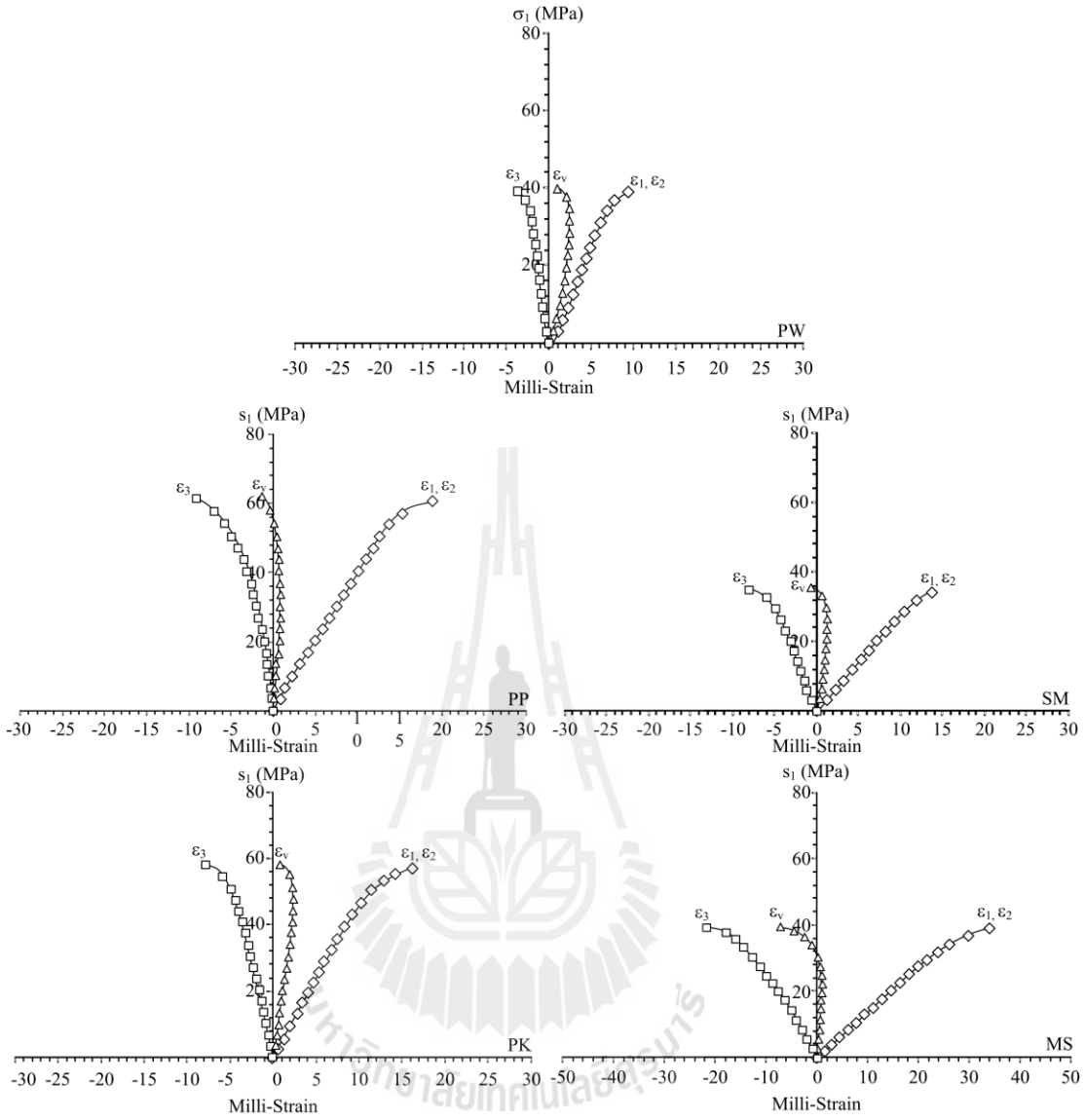

Figure 6.3 Stress-strain curves of biaxial compression test using biaxial load frame.

6.2.4 Biaxial compression test using UBC

The biaxial compressive strengths are determined using the UBC. The biaxial strengths using the UBC for the PW, PP, PK, SM and MS are 39.9 ± 1.2, 59.8 ± 1.1, 57.1 ± 1.9, 33.5 ± 1.2 and 36.5 ± 0.9 MPa, respectively. The stress-strain curves are plotted in Figure 6.4. The elastic moduli are 11.2, 10.4, 12.1, 24.8 and 20.2 GPa, respectively.

The failure specimens are combination of compressive shear and splitting tension modes, as shown in Figures 6.5. Table 6.1 summarizes compressive strength data for PW, PP, PK, SM and MS. The failure compressive strengths with standard deviation are shown in Figure 6.6 and 6.7. The elastic modulus and Poisson's ratio are calculated. The measured sample deformations are used to determine the strains along the intermediate principal axes during loading. The elastic modulus and Poisson's ratio are shown in Table 6.2.

The calculations of the Poisson's ratios and tangent elastic moduli are made at 50% of the maximum principal stress. The results of uniaxial compressive strength tests are used to calculate the elastic parameters of the rock specimens. The longitudinal strain can be measured by monitors the change in the displacement.

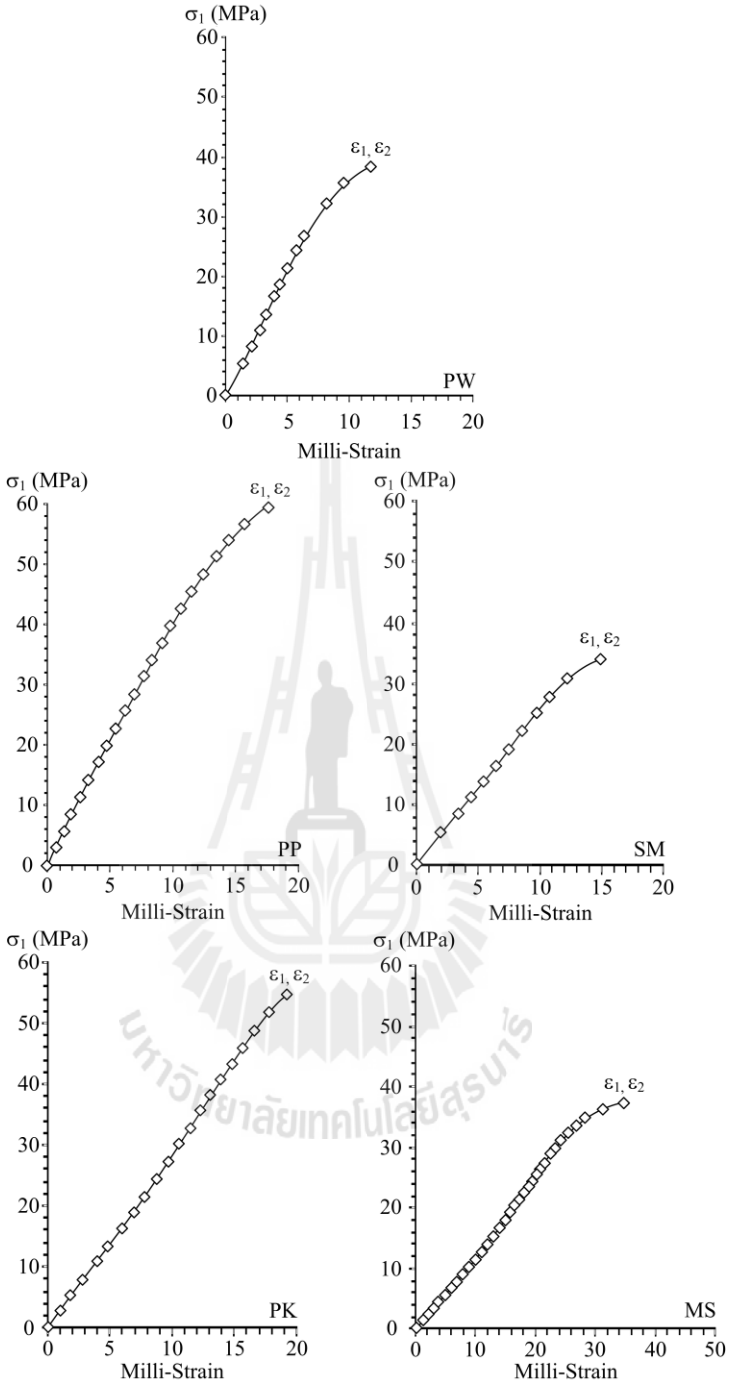

Figure 6.4 Stress-strain curves from biaxial compressive strength test using UBC.

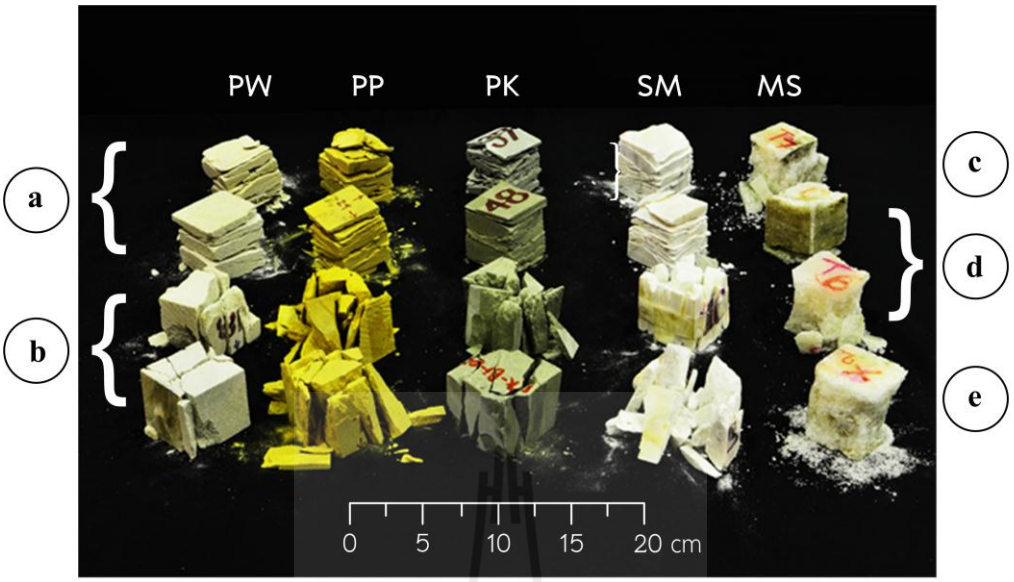

Tests

a Uniaxial compressive strength

b Biaxial compressive strength

Devices

c Conventional uniaxial load frame

d UBC

e Conventional biaxial load frame

Figure 6.5 Some post-test specimens of five rock types.

Table 6.1 Summary of compressive strength test results.

Test method	Rock types strength (MPa)				
	PW	**PP**	**PK**	**SM**	**MS**
1. Uniaxial compressive strength test using conventional frame	23.4 ±1.2	32.3 ±1.9	31.8 ±2.2	22	21.9 ±1.9
2. Uniaxial compression test using UBC	21.1 ±1.5	33.4 ±1.5	30.7 ±0.5	24.7 ±1.1	21.7 ±0.9
3. Biaxial compressive strength test using conventional frame	39	59 ±1.4	57.7 ±1.2	34	37.9 ±0.6
4. Biaxial compression test using UBC	39.9 ±1.2	59.8 ±1.1	57.1 ±1.9	33.5 ±1.2	36.5 ±0.9

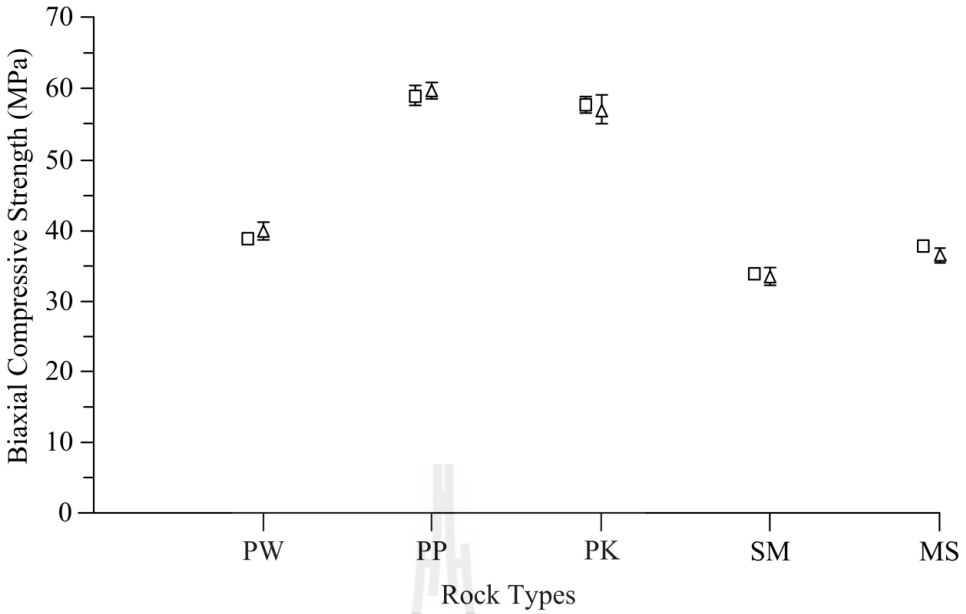

Figure 6.6 Uniaxial compressive strengths of 5 rock types obtained by using the conventional device (□) and load converter (Δ).

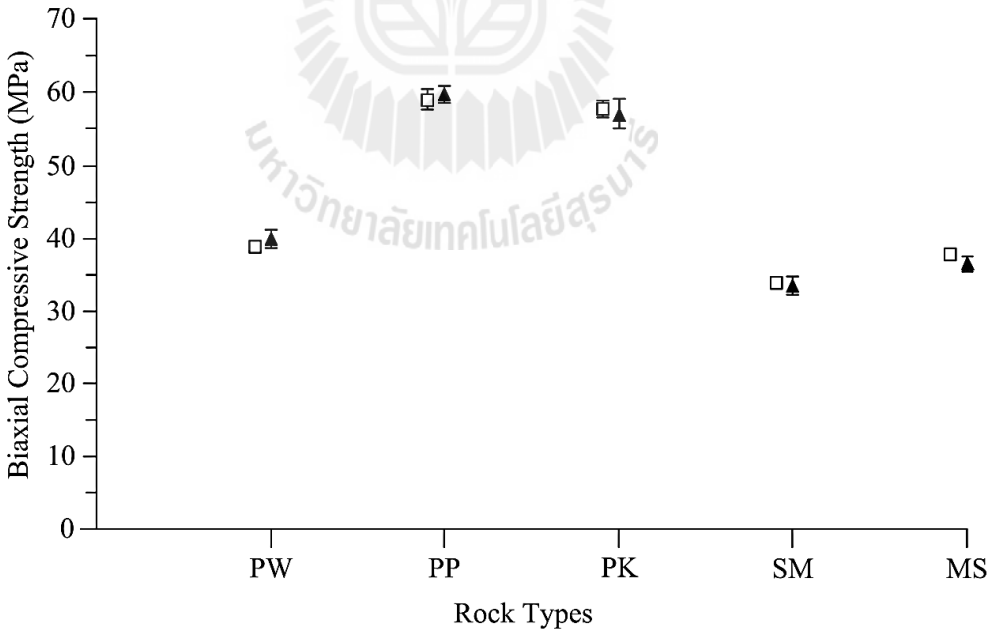

Figure 6.7 Biaxial compressive strengths of 5 rock types obtained by using the conventional device (□) and load converter (▲).

Table 6.2 The elastic modulus and Poisson's ratio of uniaxial and biaxial compressive strength tests from UBC and conventional load frame.

Tests	Devices	PW		PP		PK		SM		MS	
		E (GPa)	**ν**	**E (GPa)**	**ν**	**E (GPa)**	**ν**	**E (GPa)**	**ν**	**E (GPa)**	**ν**
Uniaxial	Conventional frame	11.3	0.30	11.4	0.32	10.3	0.26	25.1	0.18	21.6	0.40
	UBC	11.9	0.28	11.5	0.35	10.4	0.23	25.5	0.18	20.7	0.39
Biaxial	Conventional frame	11.7	-	11.2	0.33	11.9	0.26	25.0	-	20.2	0.43
	UBC	11.2	-	10.4	-	12.1	-	24.8	-	20.3	-

For the uniaxial test calculation the elastic parameters are determined by

$$\varepsilon = - \Delta L/L \tag{6.1}$$

where ε is strain

ΔL is relative shortening of the specimen length

L is length of specimen

The Young's modulus of the specimen is calculated by

$$E = \sigma / \varepsilon \tag{6.2}$$

where σ is maximum uniaxial stress

ε is longitudinal strain

The biaxial compression test ($\sigma_1 = \sigma_2$ and $\sigma_3 = 0$) results are used to calculate the elastic parameters by the following equations (Jaeger and Cook, 1979):

$$\varepsilon_1 = \sigma_1/E - \nu\sigma_2/E \quad (6.3)$$

$$\varepsilon_2 = \sigma_2/E - \nu\sigma_1/E \quad (6.4)$$

$$\varepsilon_3 = -\nu\sigma_1/E - \nu\sigma_2/E \quad (6.5)$$

The elastic parameters are calculated by

$$E = \sigma_1/\varepsilon_1 - \nu\sigma_2/\varepsilon_1 \quad (6.6)$$

or

$$E = -\nu\sigma_1/\varepsilon_3 - \nu\sigma_2/\varepsilon_3 \quad (6.7)$$

$$\nu = [\sigma_2/\varepsilon_1 - \sigma_1/\varepsilon_2] / [\sigma_1/\varepsilon_1 - \sigma_2/\varepsilon_2] \quad (6.8)$$

where ε_1 is maximum principal strain

ε_2 is intermediate principal strain

ε_3 is minor principal strain

σ_1 is maximum principal stress

σ_2 is intermediate principal stress

E is elastic modulus

ν is Poisson’s ratio

CHAPTER VII

DISCUSSIONS, CONCLUSIONS AND RECOMMENDATIONS FOR FUTURE STUDIES

7.1 Discussions and conclusions

The uniaxial-to-biaxial load converter (UBC) has been developed to determine the biaxial compressive strength and deformability of rock specimens. The proposed device has been designed and fabricated for use with most commercially available compression loading frames. The laboratory tests have been carried out to assess the performance of the UBC by determining the uniaxial and biaxial compressive strengths, elastic modulus and Poisson's ratio of cubical rock specimens with nominal dimensions of 50×50×50 mm^3. The specimens are prepared from Phra Wihan, Phu Phan and Phu Kradung sandstones, Saraburi marble and Maha Sarakham salt. The specimen deformations are monitored along the three principal directions to develop stress-strain curves from start loading until failure. The strengths and elastic parameters obtained from the UBC agree well with those from the conventional uniaxial and biaxial load frames. This indicates that the UBC design is suitable for determining the biaxial strengths of rocks under uniform two-dimensional stress ($\sigma_1=\sigma_2$, $\sigma_3=0$). The results are of useful to assess the mechanical stability of rock at the opening wall at great depth. The new device has advantage over the conventional load frame that it is less expensive and easy to operate. It also ensures that the two perpendicular biaxial stresses are always equal from start loading to failure.

The elastic parameters are one of the important parameters for design and stability analysis of the geological structures in host rocks for tunnels and underground mines. For underground openings the effects of the confining pressures at the opening boundaries on those properties can be simulated in the laboratory by performing biaxial compression testing of cubical rock specimens with UBC that has been invented to obtain the biaxial strength testing in laboratory. The existing two dimensional failure criteria for brittle rocks are adequate because they are in the form that can readily be applied in the actual design and analysis of geological structures.

7.2 Recommendations for future studies

The test with the UBC should be performed on a variety of rock types with different strengths. The effect of friction at the interface between the loading platen and rock surfaces should be investigated. Size effect on the rock biaxial strength should also be examined. The effect of temperature should be considered on the true biaxial compressive test.

REFERENCES

Alexeev, A. D., Revva, V.N., Alyshev, N.A. and Zhitlyonok, D.M. (2004). True triaxial loading apparatus and its application to coal outburst prediction. **International Journal of Coal Geology**. 58(4): 245-250.

Alsayed, M.I. (2002). Utilising the hoek triaxial cell for multiaxial testing of hollow rock cylinders. **International Journal of Rock Mechanics and Mining Sciences**. 39(3): 355-366.

ASTM D 7012-04 (2010). Standard test method for compressive strength and elastic moduli of intact rock core specimens under varying states of stress and temperatures. In **Annual Book of ASTM Standards** (Vol. 04.09). Philadelphia: American Society for Testing and Materials.

Bobet, A. and Einstein, H.H. (1998). Fracture coalescence in rock-type materials under uniaxial and biaxial compression. **International Journal of Rock Mechanics & Mining Sciences**. 47(7): 863-888.

Brown, E. T. (1981). Rock Characterization Testing and Monitoring: ISRM suggested methods. The commission on rock testing method. **International Society of Rock Mechanics**, Pergamon Press.

Cai, M. (2008). Influence of intermediate principal stress on rock fracturing and strength near excavation boundaries-Insight from numerical modeling. **International Journal of Rock Mechanics & Mining Sciences**. 45: 763-772.

Chang, C. and Haimson, B. (2005). Non-dilatant deformation and failure mechanism in two Long Valley Caldera rocks under true triaxial compression. **International Journal of Rock Mechanics & Mining Sciences**. 42: 402–414.

Colmenares, L.B. and Zoback, M.D., (2002). A statistical evaluation of intact rock failure criteria constrained by polyaxial test data for five different rocks. **International Journal of Rock Mechanics & Mining Sciences**. 39: 695-729.

Fakhimi, A., Carvalho, F., Ishida, T. and Labuz, J.F. (2002). Simulation of failure around a circular opening in rock. **International Journal of Rock Mechanics & Mining Sciences**. 39: 507-515.

Haimson, B. (2006). True triaxial stresses and the brittle fracture of rock. **Pure and Applied Geophysics**. 163: 1101–1113.

Haimson, B. and Chang, C. (2000). A new true triaxial cell for testing mechanical properties of rock, and its use to determine rock strength and deformability of Westerly granite. **International Journal of Rock Mechanics & Mining Sciences**. 37(1-2): 285-296.

Handin, J., Heard, H.C. and Magouirk, J.N. (1967). Effect of the intermediate principal stress on failure of limestone, dolomite, and glass at different temperature and strain rate. **Journal of Geophysical Research**. 72(2): 611-640.

Hibbeler, R. C. (2008). **Mechanics of Materials**. Singapore: Prentice-Hall, Inc. 910 pp.

Hibbeler, R. C. (2010). **Engineering Mechanics Statics**. Singapore: Prentice-Hall, Inc. 655 pp.

Hoek, E., and Brown, E.T. (1988). The Hoek-Brown failure criterion – a1988 update. In **Proceedings of the 15th Canadian Rock Mechanics Symposium**. Toronto, Canada. pp. 31–38.

Hoek, E., and Franklin, J.A, (1970). Developments in triaxial testing equipment. **Rock Mechanics**. 2: 223-228.

Jaeger, J.C., and Cook, N.G.W. (1979). **Fundamentals of Rock Mechanics** (3rd. Edn.), Chapman & Hall, London, pp. 105-106.

Kemthong, R. and Fuenkajorn, K. (2007). Prediction of joint shear strengths of ten rock types using field-identified parameters. In **Proceedings 1st Thailand Symposium on Rock Mechanics**. Nakhon Ratchasima, Thailand. 1: 195-209.

Kulatilake, P.H., Park, J. and Malama, B. (2006). A new rock mass failure criterion for biaxial loading conditions. **Geotechnical and Geological Engineering**. 24: 871-888.

Kwasniewski, M., Takahashi, M., and Li, X. (2003). Volume changes in sandstone under true triaxial compression conditions. **ISRM 2003–Technology Roadmap for Rock Mechanics**. South African Institute of Mining and Metallurgy. pp. 683-688.

Mogi, K. (1967). Effect of the intermediate principal stress on rock failure. **Journal of Geophysical Research**. 72(20): 5117-5131.

Mogi, K. (1971). Fracture and flow of rocks under high triaxial compression. **Journal of Geophysical Research**. 76(5): 1255-1269.

Murrell, S.A.F. (1963). A criterion for brittle fracture of rocks and concrete under triaxial stress, and the effect of pore pressure on the criterion. In **Proceedings 5th Symposium on Rock Mechanics**. Minnesota, USA. pp. 563-577.

Rao, K.S. and Tiwari, R.P. (2002). Physical simulation of jointed model materials under biaxial and true triaxial stress states. In **Research Report**, IIT Delhi, India. p. 30.

Sagong, M., Park, D., Yoo, J. and Lee, J.S. (2011). Experimental and numerical analyses of an opening in a jointed rock mass under biaxial compression. **International Journal of Rock Mechanics and Mining Sciences**. 48(7): 1055-1067.

Sahouryeh, E., Dyskin, A.V. and Germanovich, L.N. (2002). Crack growth under biaxial compression. **Engineering Fracture Mechanics**. 69(18): 2187-2198.

Sibai, M., Henry, J.P. and Gros, J.C. (1997). Hydraulic fracturing stress measurement using a true triaxial apparatus. **International Journal of Rock Mechanics and Mining Sciences**. 34(3-4): 289.e1-289.e10.

Song, I. and Haimson, B.C. (1997). Polyaxial strength criteria and their use in estimating in situ stress magnitudes from borehole breakout dimensions. **International Journal of Rock Mechanics and Mining Sciences**. 34(3-4): 116.e1-116.e16.

Sriapai, T. (2010). **True triaxial compressive strengths of Maha Sarakham rock salt**. M.S. thesis, Suranaree University of Technology, Thailand. p. 22.

Sriapai, T., Samsri, P. and Fuenkajorn, K. (2011). Polyaxial strengths of Maha Sarakham salt. In **Proceedings 3rd Thailand Symposium on Rock Mechanics**. Phetchaburi, Thailand. 3: 79-87.

Thosuwan, R. (2009). **Development of true triaxial load frame using cantilever system**. M.S. thesis, Suranaree University of Technology, Thailand. p. 34.

Tiwari, R.P. and Rao, K.S. (2004). Physical modeling of a rock mass under a true triaxial stress state. **International Journal of Rock Mechanics and Mining Sciences**. 41(3): 1-6.

Tiwari, R.P. and Rao, K.S. (2006). Post failure behavior of a rock mass under the influence of triaxial and true triaxial confinement. **Engineering Geology**. 84: 112-129.

Walsri, C., Poonprakon, P., Thosuwan, R. and Fuenkajorn, K. (2009). Compressive and tensile strengths of sandstones under true triaxial stresses. In **Proceedings of the 2nd Thailand Symposium on Rock Mechanics**. Chonburi, Thailand. 2: 199-218.

Wawersik, W.R., Carlson, L.W., Holcomb D. J. and Williams, R.J. (1997). New method for true-triaxial rock testing. **International Journal of Rock Mechanics and Mining Sciences**. 34(3): 365-365.

Wiebols, G.A. and Cook, N.G.W. (1968). An energy criterion for the strength of rock in polyaxial compression. **International Journal of Rock Mechanics and Mining Sciences**. 5(6): 529-549.

Yun, X., Mitri, H.S., Yang, X. and Wang, Y. (2010). Experimental investigation into biaxial compressive strength of granite. **International Journal of Rock Mechanics & Mining Sciences**. 47(2): 334-341.

Zhu, W.C., Liu, J., Tang, C.A., Zhao, X.D. and Brandy, B.H. (2005). Simulation of progresses around underground excavations under biaxial compression. **Tunnelling and Underground Space Technology**. 20(3): 231-247.